

## Glutaminase and poly(ADP-ribose) polymerase inhibitors suppress pyrimidine synthesis and *VHL*-deficient renal cancers

Arimichi Okazaki, ... , Lee Zou, Othon Iliopoulos

*J Clin Invest.* 2017;127(5):1631-1645. <https://doi.org/10.1172/JCI87800>.

Research Article

Metabolism

Oncology

Many cancer-associated mutations that deregulate cellular metabolic responses to hypoxia also reprogram carbon metabolism to promote utilization of glutamine. In renal cell carcinoma (RCC), cells deficient in the von Hippel–Lindau (*VHL*) tumor suppressor gene use glutamine to generate citrate and lipids through reductive carboxylation (RC) of  $\alpha$ -ketoglutarate ( $\alpha$ KG). Glutamine can also generate aspartate, the carbon source for pyrimidine biosynthesis, and glutathione for redox balance. Here we have shown that *VHL*<sup>-/-</sup> RCC cells rely on RC-derived aspartate to maintain de novo pyrimidine biosynthesis. Glutaminase 1 (GLS1) inhibitors depleted pyrimidines and increased ROS in *VHL*<sup>-/-</sup> cells but not in *VHL*<sup>+/+</sup> cells, which utilized glucose oxidation for glutamate and aspartate production. GLS1 inhibitor-induced nucleoside depletion and ROS enhancement led to DNA replication stress and activation of an intra-S phase checkpoint, and suppressed the growth of *VHL*<sup>-/-</sup> RCC cells. These effects were rescued by administration of glutamate,  $\alpha$ KG, or nucleobases with *N*-acetylcysteine. Further, we observed that the poly(ADP-ribose) polymerase (PARP) inhibitor olaparib synergizes with GLS1 inhibitors to suppress the growth of *VHL*<sup>-/-</sup> cells in vitro and in vivo. This work describes a mechanism that explains the sensitivity of RCC tumor growth to GLS1 inhibitors and supports the development of therapeutic strategies for targeting *VHL*-deficient RCC.

Find the latest version:

<https://jci.me/87800/pdf>



# Glutaminase and poly(ADP-ribose) polymerase inhibitors suppress pyrimidine synthesis and *VHL*-deficient renal cancers

Arimichi Okazaki,<sup>1,2,3</sup> Paulo A. Gameiro,<sup>1,3,4</sup> Danos Christodoulou,<sup>1,3,4</sup> Laura Laviollette,<sup>1,3,4</sup> Meike Schneider,<sup>1,3,4</sup> Frances Chaves,<sup>5</sup> Anat Stemmer-Rachamimov,<sup>4,5</sup> Stephanie A. Yazinski,<sup>1,4</sup> Richard Lee,<sup>3,4</sup> Gregory Stephanopoulos,<sup>6</sup> Lee Zou,<sup>1,4</sup> and Othon Iliopoulos<sup>1,3,4</sup>

<sup>1</sup>Center for Cancer Research at Massachusetts General Hospital Cancer Center, Charlestown, Massachusetts, USA. <sup>2</sup>Nitto Denko Corp., Osaka, Japan. <sup>3</sup>Division of Hematology-Oncology, Department of Medicine, Massachusetts General Hospital, Boston, Massachusetts, USA. <sup>4</sup>Harvard Medical School, Boston, Massachusetts, USA. <sup>5</sup>Molecular Pathology Unit, Massachusetts General Hospital, Boston, Massachusetts, USA. <sup>6</sup>Department of Chemical Engineering, Massachusetts Institute of Technology, Cambridge, Massachusetts, USA.

Many cancer-associated mutations that deregulate cellular metabolic responses to hypoxia also reprogram carbon metabolism to promote utilization of glutamine. In renal cell carcinoma (RCC), cells deficient in the von Hippel-Lindau (*VHL*) tumor suppressor gene use glutamine to generate citrate and lipids through reductive carboxylation (RC) of  $\alpha$ -ketoglutarate ( $\alpha$ KG). Glutamine can also generate aspartate, the carbon source for pyrimidine biosynthesis, and glutathione for redox balance. Here we have shown that *VHL*<sup>-/-</sup> RCC cells rely on RC-derived aspartate to maintain de novo pyrimidine biosynthesis. Glutaminase 1 (GLS1) inhibitors depleted pyrimidines and increased ROS in *VHL*<sup>-/-</sup> cells but not in *VHL*<sup>+/+</sup> cells, which utilized glucose oxidation for glutamate and aspartate production. GLS1 inhibitor-induced nucleoside depletion and ROS enhancement led to DNA replication stress and activation of an intra-S phase checkpoint, and suppressed the growth of *VHL*<sup>-/-</sup> RCC cells. These effects were rescued by administration of glutamate,  $\alpha$ KG, or nucleobases with *N*-acetylcysteine. Further, we observed that the poly(ADP-ribose) polymerase (PARP) inhibitor olaparib synergizes with GLS1 inhibitors to suppress the growth of *VHL*<sup>-/-</sup> cells in vitro and in vivo. This work describes a mechanism that explains the sensitivity of RCC tumor growth to GLS1 inhibitors and supports the development of therapeutic strategies for targeting *VHL*-deficient RCC.

## Introduction

Hypoxia is a hallmark of human cancer. Tumor-associated hypoxia activates multiple cellular programs that promote adaptation of a tumor to its microenvironment, where oxygen and nutrient availability are restricted. Hypoxia reprograms cancer cell metabolism to circumvent some of these shortages and endow cancer cells with a proliferative advantage (1, 2). The cellular metabolic response to hypoxia is in major part orchestrated by HIF-1 $\alpha$  and HIF-2 $\alpha$ . These transcriptional factors enhance glycolysis and mitigate glucose oxidation in the mitochondria, thus supporting cell proliferation under hypoxia (3–6). While enforcing anaerobic glycolysis, HIF-1 $\alpha$ /2 $\alpha$  and cancer-associated mutations that deregulate hypoxia signaling mediate a complementary metabolic switch to a glutamine-maintained TCA cycle, through the activation of reductive carboxylation (RC) of  $\alpha$ -ketoglutarate ( $\alpha$ KG), a metabolic reaction that is heavily used to maintain de novo lipogenesis under hypoxia (7–9). Human clear cell renal cell carcinomas (RCCs) are driven by HIF-2 $\alpha$ , due to mutational inactivation of the von Hippel-Lindau (*VHL*) tumor suppressor gene, and provide a cancer model for studying reprogramming of metabolism by hypoxia signaling (7, 10, 11). Using *VHL*<sup>-/-</sup> cell lines, we showed

that it is the expression of HIF-2 $\alpha$  that promotes the reductive phenotype of RCC cells both in vitro and in vivo, rendering RCC cells dependent on glutamine metabolism (10).

There is compelling evidence that, in addition to hypoxia, many cancer-associated mutations directly reprogram the central carbon metabolism and promote increased glutamine utilization for biomass and reducing equivalent production (12–14). Such a cancer metabolic reprogramming is not uniform but rather cell type and “driver” mutation specific. For example, the *c-myc* oncogene promotes glutaminolysis (15), by transcriptionally repressing the glutaminase 1-targeting miR-23a/b (16, 17). Activated K-Ras promotes glutamine-derived aspartate formation in a mouse model of pancreatic cancer (18), while supporting purine nucleotide synthesis by funneling glucose into the pentose phosphate pathway (19). WT p53 and HER2 upregulate the transcription of glutaminase 2 and glutaminase 1 (GLS1) correspondingly (20, 21).

Glutamine metabolism is not only used by cancer cells to circumvent stress induced by tumor microenvironment but can also contribute to resistance to targeted therapy. For example, activation of mTORC1 as a result of cancer-associated mutations promotes glutamine anaplerosis by repressing *SIRT4* transcription and thus activating glutamate dehydrogenase (22). Reversely, treatment of glioblastoma tumors with mTOR inhibitors resulted in upregulation of GLS1 expression and enhanced utilization of glutamine (23). Lastly, upregulated transport of glutamine through the SLC1A5 and SLC38A2 cell surface car-

**Conflict of interest:** The authors have declared that no conflict of interest exists.

**Submitted:** March 31, 2016; **Accepted:** January 26, 2017.

**Reference information:** *J Clin Invest.* 2017;127(5):1631–1645.

<https://doi.org/10.1172/JCI87800>.

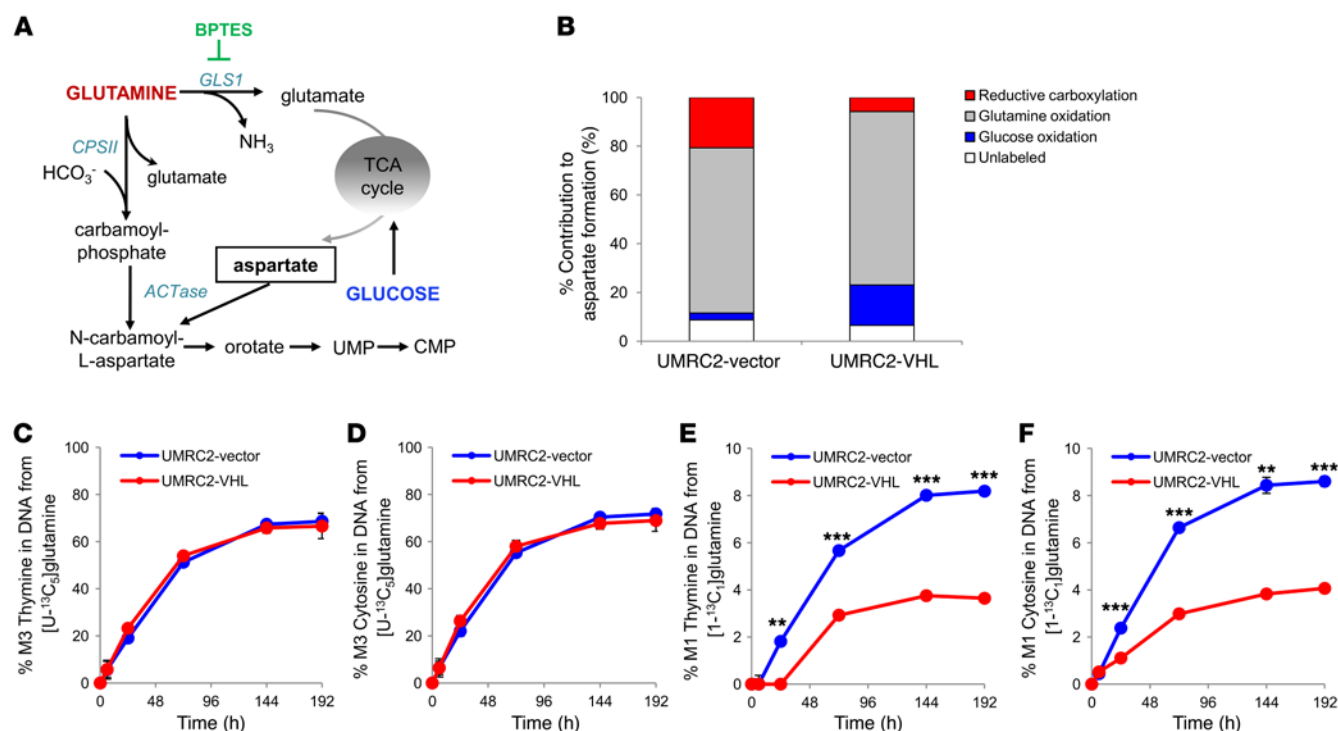


**Figure 1. Biosynthesis of DNA pyrimidines from glutamine carbons in RCC cells.** (A) Diagram depicting the contribution of glutamine and glucose to the formation of aspartate and downstream intermediates of pyrimidine nucleosides, and the inhibition of GLS1 by BPTES. (B) Contribution of the different source pathways to the formation of aspartate. One representative experiment is shown, in which an isogenic pair of *VHL*<sup>-/-</sup> and *VHL*<sup>+/-</sup> UMRC2 cells was labeled with [U-<sup>13</sup>C]<sub>6</sub>glucose, [U-<sup>13</sup>C]<sub>5</sub>glutamine, or [1-<sup>13</sup>C]<sub>5</sub>glutamine for 24 hours; the M0 obtained using the [U-<sup>13</sup>C]<sub>5</sub>glutamine tracer was used to depict the “unlabeled” fraction of aspartate. (C and D) Using [U-<sup>13</sup>C]<sub>5</sub>glutamine, the time course (8 days) shows the <sup>13</sup>C enrichment of thymine (C), and cytosine (D), determined from column-purified and formic acid-hydrolyzed DNA. (E and F) Using [1-<sup>13</sup>C]<sub>5</sub>glutamine, the time course (8 days) shows the incorporation of the <sup>13</sup>C label on DNA-derived thymine (E) and cytosine (F). Error bars represent SEM (*n* = 3). Student’s *t* test with Bonferroni correction (to account for multiple comparisons) compared *VHL*<sup>-/-</sup> to *VHL*<sup>+/-</sup> cells in E and F. \*\**P* < 0.01, \*\*\**P* < 0.001. GLS1, glutaminase 1; CPSII, carbamoyl phosphate synthetase II; ACTase, aspartate transcarbamoylase; OMP, orotidine monophosphate; UMP, uridine monophosphate; PRPP, 5-phosphoribosyl pyrophosphate.

riers can promote resistance of breast cancer cells to treatment with paclitaxel in vitro and in vivo (24).

Despite the proliferating evidence of the contribution of glutamine to cancer cell survival, data on the biochemical mechanisms that mediate repression of cell growth by glutamine deprivation are scant. Simon’s group provided early significant insights by showing that glutamine depletion in MYC-transformed cells induces apoptosis through ATF4-dependent, but p53-independent, PUMA and NOXA induction (25).

Here we provide additional insights into the mechanisms by which GLS1 inhibition represses RCC cancer cell growth and highlight a putative strategy to enhance this effect. Glutamine-derived carbons, besides being a source of lipogenic acetyl-CoA in cancer cells, can also be used in the TCA cycle to generate aspartate, the carbon source for de novo pyrimidine nucleotide synthesis (26, 27). Given that loss of *VHL* promotes glutamine utilization for biomass production, including pyrimidines, we sought to investigate how *VHL*<sup>-/-</sup> (and therefore HIF-1 $\alpha$ /2 $\alpha$ -expressing) human RCC cells redirect glucose and glutamine to maintain de novo pyrimidine biosynthesis. Using <sup>13</sup>C tracers and employing GLS1 inhibitors as tool compounds, we showed that *VHL*-deficient RCC cells depend on RC-derived aspartate to maintain de novo pyrimidine synthesis in a HIF-dependent manner. GLS1 inhibitors lower the reductive transition of glutamine carbons to aspartate

and result in decreased de novo synthesis of pyrimidines. Therefore, *VHL*<sup>-/-</sup> cells treated with GLS1 inhibitors fail to synthesize adequate nucleotides and display DNA replication stress associated with cell growth suppression. In addition to being a carbon source for pyrimidines, glutamine carbons are also utilized for glutathione (GSH) synthesis. We showed that GLS1 inhibitors increase intracellular ROS through suppression of GSH biosynthesis. Enhancement of ROS induces DNA replication stress independently from suppressed pyrimidine synthesis. The acquisition of a DNA replication stress phenotype renders the RCC cells sensitive to poly(ADP-ribose) polymerase (PARP) inhibitors. Importantly, combination of GLS1 inhibitors with olaparib has a synergistic effect in selectively suppressing the growth of *VHL*<sup>-/-</sup> RCC cells in vitro and in vivo. These results describe a mechanism that explains, at least in part, the sensitivity of RCC cells to GLS1 inhibitors and set the foundation for combination treatment of GLS1 inhibitors with olaparib for RCC and other *VHL*<sup>-/-</sup> tumors.

## Results

*RC contributes to DNA synthesis via production of aspartate in VHL-deficient human RCC cells.* In mammalian cells, uridine monophosphate (UMP) is the common precursor for pyrimidine-containing nucleotides, being synthesized de novo from 5-phosphoribosyl pyrophosphate (PRPP, produced from ribose 5-phosphate),

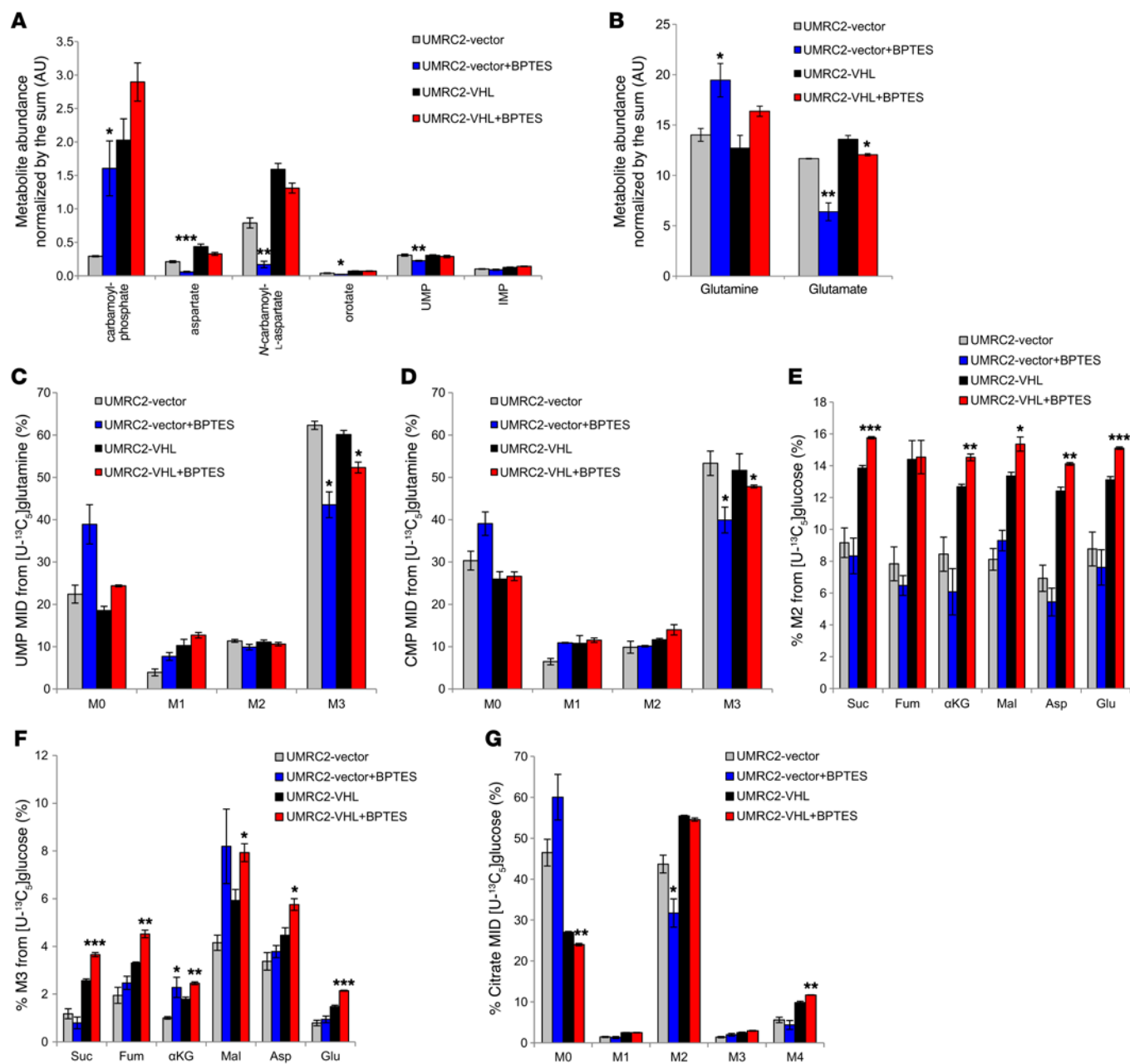


**Figure 2. Inhibition of GLS1 decreases intracellular aspartate and selectively suppresses de novo pyrimidine synthesis in *VHL*<sup>-/-</sup> cells.** (A and B) Isogenic *VHL*<sup>-/-</sup> and *VHL*<sup>+/+</sup> UMRC2 cells were cultured in the absence or presence of 1.5 μM BPTES for 48 hours, and the metabolites were analyzed by LC-MS/MS. (A) Effect of BPTES on the levels of pyrimidine nucleotides and their intermediates. (B) Effect of BPTES on the levels of glutamine and glutamate in the isogenic pair of UMRC2 cells. Metabolite levels were normalized to the sum of 288 metabolites obtained from extracts in the corresponding cell type. (C and D) The pair of UMRC2 cells was labeled with [U-<sup>13</sup>C]<sub>5</sub>]glutamine in the absence or presence of 2 μM BPTES for 48 hours, and the metabolite enrichment was measured by LC-MS/MS. Effect of BPTES on the <sup>13</sup>C enrichment of UMP (C) and CMP (D) is shown. (E–G) The pair of UMRC2 cells were labeled with [U-<sup>13</sup>C]<sub>6</sub>]glucose with or without 2 μM BPTES for 48 hours, and the metabolite enrichment was measured by GC-MS. Effect of BPTES on the contribution of glucose oxidation, determined by the level of M2-enriched (E) and M3-enriched (F) TCA cycle intermediates, and of citrate enrichment (G). Error bars represent SEM (n = 3). Student's *t* test compared BPTES-treated with corresponding control cells in B–G. \**P* < 0.05, \*\**P* < 0.01, \*\*\**P* < 0.001. MID, Mass Isotopomer Distribution; Suc, succinate; Fum, fumarate; αKG, α-ketoglutarate; Mal, malate; Asp, aspartate; Glu, glutamate.

glutamine-derived nitrogens, and aspartate. The pathway consists of 6 enzymatic steps: carbamoyl-phosphate synthetase II (CPSII), aspartate transcarbamoylase (ACTase), dihydroorotase, dihydroorotate dehydrogenase, orotate phosphoribosyltransferase, and orotidine monophosphate decarboxylase (28). CAD is the trifunctional enzyme that comprises the CPSII, ACTase, and dehydro-

orotase steps of UMP synthesis, and its activity is allosterically regulated at multiple levels to mediate de novo pyrimidine biosynthesis in a cell cycle-dependent manner (27, 29, 30). During the de novo synthesis of pyrimidines in mammalian cells, glutamine donates the amide nitrogen to bicarbonate, forming *N*-carbamoyl-phosphate via CPSII. In turn, *N*-carbamoyl-phosphate com-

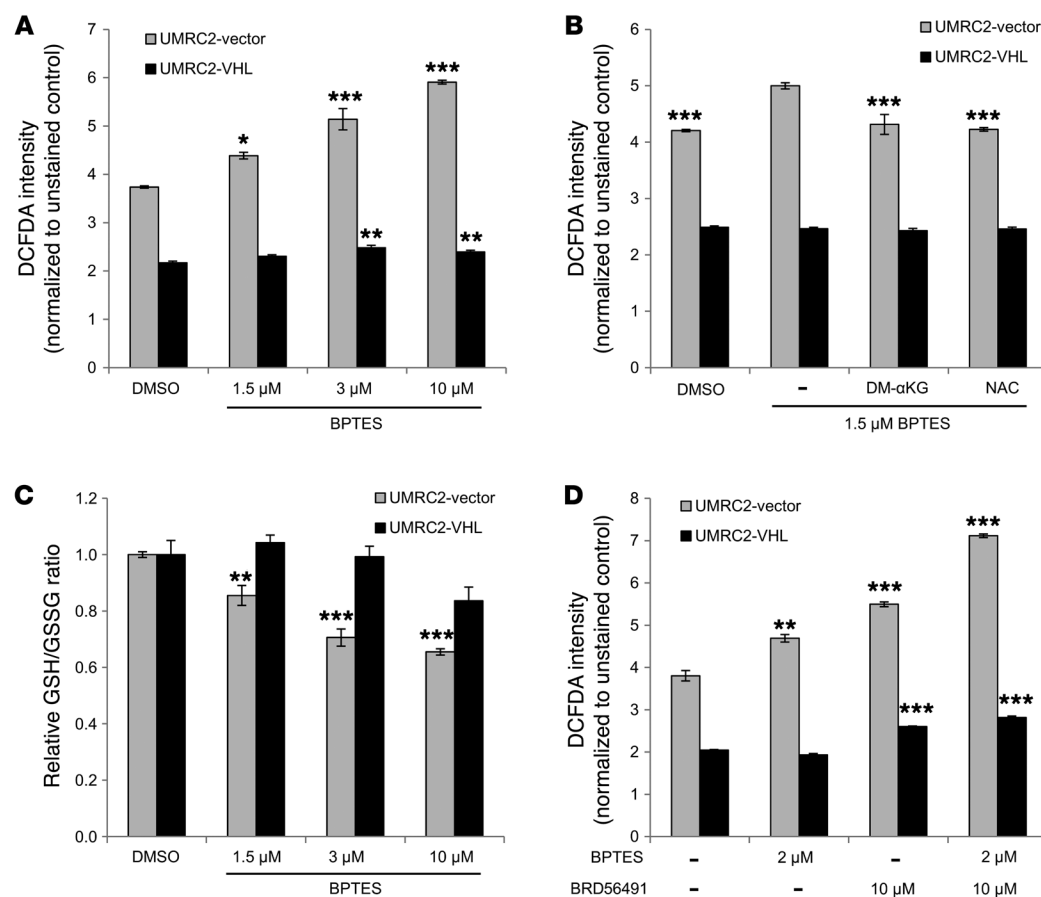


**Figure 3. Inhibition of GLS1 selectively increases intracellular ROS levels in *VHL*<sup>-/-</sup> RCC cells.** (A) Intracellular ROS levels were determined by carboxy-DCFDA staining in *VHL*<sup>-/-</sup> and *VHL*<sup>+/+</sup> UMR2 cells treated with 1.5, 3, and 10 μM BPTES for 24 hours. The DCFDA intensities were normalized to corresponding unstained control. (B) Rescue effects of exogenous dimethyl  $\alpha$ -ketoglutarate (DM- $\alpha$ KG, 0.5 mM) and *N*-acetylcysteine (NAC, 4 mM) on intracellular ROS level in *VHL*<sup>-/-</sup> and *VHL*<sup>+/+</sup> UMR2 cells treated with 1.5 μM BPTES for 24 hours. (C) GSH/GSSG ratios were determined in *VHL*<sup>-/-</sup> and *VHL*<sup>+/+</sup> UMR2 cells treated with 1.5, 3, and 10 μM BPTES for 24 hours. (D) A small-molecule ROS enhancer, BRD56491, synergistically enhanced intracellular ROS levels with BPTES in *VHL*<sup>-/-</sup> UMR2 cells. Error bars represent SEM ( $n = 3$ ). \* $P < 0.05$ , \*\* $P < 0.01$ , \*\*\* $P < 0.001$ , Dunnett's test against corresponding control conditions.

bins with aspartate to form *N*-carbamoyl-L-aspartate through ACTase, which is further modified and combined with PRPP to produce orotidine monophosphate and, after a decarboxylation step (which releases the carbon [C1] of aspartate), UMP (Figure 1A and Supplemental Figure 1; supplemental material available online with this article; <https://doi.org/10.1172/JCI87800DS1>). Therefore, aspartate contributes with 3 carbons to the synthesis of UMP and to the other pyrimidine nucleotides. Aspartate is produced from transaminated oxaloacetate, which can be generated from 3 distinct sources: (a) glutamine-derived carbons only (through glutamine oxidation in the first round of the TCA cycle), (b) RC, in which case it is also composed exclusively by glutamine carbons, or (c) through several rounds of the TCA cycle via the combined action of pyruvate dehydrogenase or pyruvate carboxylase, and glutamine anaplerosis, being formed from both glucose carbons and glutamine carbons. We will describe glucose oxidation as pathway (d), since it requires the continuous supply of 2 glucose or 3 glucose carbons.

To study the de novo synthesis of pyrimidine in RCC cells, we used a system of isogenic RCC UMR2 cells that are *VHL*-deficient (HIF-expressing) and reconstituted either with a pBABE control vector (termed *VHL*<sup>-/-</sup>) or with WT *VHL* (termed *VHL*<sup>+/+</sup>), as previously described (10). We cultured the pair of *VHL*<sup>-/-</sup> and *VHL*<sup>+/+</sup> cells in the presence of <sup>13</sup>C glucose or glutamine tracers and measured the <sup>13</sup>C isotopic enrichment of aspartate and pyrimidine intermediates and in the DNA biomass. First, to quantify the contribution of the different pathways to aspartate synthesis in RCC

cells, we cultured the pair of RCC cells with <sup>13</sup>C tracers that specifically trace the contribution of the aforementioned 3 routes (Supplemental Figure 2), and observed that the contribution of these pathways is different between *VHL*<sup>-/-</sup> and *VHL*<sup>+/+</sup> UMR2 cells (Figure 1B). While we acknowledge that most of the aspartate is formed from glutamine oxidation in both cell types (determined by the degree of M4 enrichment from [U-<sup>13</sup>C<sub>5</sub>]glutamine), there was a significant difference between the contribution of glucose oxidation (determined by the degree of M2 and M3 enrichment from [U-<sup>13</sup>C<sub>6</sub>]glucose) and that of RC (determined by the degree of M1 enrichment from [1-<sup>13</sup>C<sub>1</sub>]glutamine) between *VHL*<sup>-/-</sup> and *VHL*<sup>+/+</sup> UMR2 cells (Figure 1B). This observation led to the hypothesis that HIF expression affects the substrate preference for de novo pyrimidine biosynthesis, and that this metabolic phenotype may be exploited to selectively inhibit this pathway in *VHL*<sup>-/-</sup> cells.

To confirm the contribution of glutamine carbons to DNA synthesis, we cultured the pair of UMR2 cells in the presence of [U-<sup>13</sup>C<sub>5</sub>]glutamine for several days and monitored the <sup>13</sup>C label incorporation in thymine and cytosine using gas chromatography/mass spectrometry (GC-MS); the free bases were obtained from isolated and hydrolyzed DNA. [U-<sup>13</sup>C<sub>5</sub>]glutamine can contribute with 3 carbons to pyrimidine biosynthesis through the TCA cycle (Figure 1A and Supplemental Figure 1, via either glutamine oxidation or RC). As seen in Figure 1, C and D, both *VHL*<sup>-/-</sup> and *VHL*<sup>+/+</sup> cells heavily rely on glutamine carbons to produce DNA bases, with little difference observed between the 2 cell types, although *VHL*<sup>+/+</sup> cells appear to incorporate the <sup>13</sup>C tracer at a higher rate

during the first 48 hours. This is consistent with the notion that de novo DNA synthesis is a readout of cell proliferation rates (31, 32), and *VHL*<sup>+/+</sup> UMRC2 cells grow slightly faster than their *VHL*<sup>-/-</sup> counterparts in vitro (although they do not form tumors in vivo). This indicates that glutamine is a major nutrient for de novo pyrimidine biosynthesis in both RCC cells, but this experiment does not distinguish the utilization of glutamine carbons via glutamine oxidation or RC. The fact that the <sup>13</sup>C incorporation is not higher in *VHL*<sup>-/-</sup> cells is not incompatible with the observed different contribution of glutamine carbons for aspartate synthesis (Figure 1B), but rather raises the possibility that both RCC cell types rely on glutamine to synthesize pyrimidines when cultured under conditions of abundant glucose and glutamine. We also detected a similar <sup>13</sup>C labeling pattern in uracil, albeit a lower signal (data not shown), possibly reflecting spontaneous deamination of cytosine during the experimental procedure (33). Next, to determine the contribution of RC to DNA synthesis, we labeled the pair of UMRC2 cells with [1-<sup>13</sup>C]<sub>1</sub>glutamine, which transfers the label to aspartate and pyrimidines specifically through RC. We observed that the <sup>13</sup>C enrichment of thymine and cytosine was higher in *VHL*<sup>-/-</sup> than in *VHL*<sup>+/+</sup> UMRC2 cells, indicating that at least 10% of DNA was synthesized through RC during the course of 8 days. Notably, the carbon (C1) of aspartate is lost during de novo pyrimidine biosynthesis, but RC transfers the <sup>13</sup>C label to aspartate in the 4 carbon (C4). However, owing to molecular symmetry of fumarate (34) and reversibility of the malate dehydrogenase and fumarate hydratase reactions, C1 and C4 can interchange and lead to partial loss of <sup>13</sup>C incorporation in pyrimidines. Thus, the observed <sup>13</sup>C enrichment of DNA is an underestimation of the actual RC contribution to DNA synthesis due to the isotopic scrambling. Overall, these results indicate that RC can contribute to DNA synthesis in RCC cells in a HIF-dependent manner.

*Glutaminase inhibition compromises de novo pyrimidine biosynthesis in VHL-deficient human RCC cells.* *N*-carbamoyl-aspartate is formed through condensation of *N*-carbamoyl-phosphate with aspartate, the latter being produced from either glucose or glutamine (Figure 1A and Supplemental Figure 1). Since glutamine-derived carbons contributed to a higher steady-state production of aspartate and DNA in *VHL*<sup>-/-</sup> than *VHL*<sup>+/+</sup> UMRC2 cells, we hypothesized that glutamine deprivation would impair pyrimidine biosynthesis selectively in *VHL*-deficient cells. To test this hypothesis, we cultured isogenic *VHL*<sup>-/-</sup> and *VHL*<sup>+/+</sup> UMRC2 cells with a GLS1 inhibitor, bis-2-(5-phenylacetamido-1,3,4-thiadiazol-2-yl) ethyl sulfide (BPTES), for 48 hours and measured the levels of the pyrimidine intermediates using liquid chromatography/tandem mass spectrometry (LC-MS/MS). Treatment with BPTES significantly decreased the levels of *N*-carbamoyl-aspartate and UMP in *VHL*<sup>-/-</sup> UMRC2 cells (Figure 2A). Consistent with the hypothesis that glutamine-derived carbons are required for aspartate synthesis, the levels of aspartate decreased in BPTES-treated *VHL*<sup>-/-</sup> cells, while *N*-carbamoyl-phosphate increased. These observations are consistent with network topology and suggest that loss of *VHL* limits RCC cells in their ability to produce aspartate under GLS1-inhibited conditions, which leads to the accumulation of *N*-carbamoyl-phosphate. In contrast, the effect induced by BPTES on metabolite pool sizes was overall significantly less pronounced in *VHL*<sup>+/+</sup> cells (Figure 2A). Treatment with BPTES increased the

levels of glutamine and reduced glutamate levels in both UMRC2 cell types (Figure 2B), confirming the expected metabolic effect of GLS1 inhibition. This effect was nevertheless less pronounced in *VHL*<sup>+/+</sup> UMRC2 cells at the level of glutamate, corroborating our previous observations that *VHL* reconstitution in *VHL*-deficient RCC cells stimulates glucose oxidation in the TCA cycle and rescues the production of glutamate from glucose carbons (10). To test whether the effect on pyrimidine synthesis induced by GLS1 inhibition is due to an impaired carbon flux to pyrimidine synthesis, we labeled the pair of UMRC2 cells with [U-<sup>13</sup>C]<sub>5</sub>glutamine for 48 hours, and measured the isotopic enrichment of UMP and CMP in the presence of BPTES. The <sup>13</sup>C enrichment of M3 UMP and CMP was decreased in both *VHL*<sup>-/-</sup> and *VHL*<sup>+/+</sup> UMRC2 cells, albeit the effect was significantly more pronounced in *VHL*<sup>-/-</sup> cells (Figure 2, C and D). As expected, there was no <sup>13</sup>C incorporation in inosine monophosphate, the precursor nucleotide for purines, whose synthesis does not require glutamine carbons (Supplemental Figure 3A); the observed minimal M1 abundance (~5%) is most likely due to the natural abundance of <sup>13</sup>C (we did not correct for the natural abundance of isotopomer enrichments in the LC-MS/MS experiments). We showed before that the levels of GLS1 are similar between *VHL*<sup>-/-</sup> and *VHL*<sup>+/+</sup> UMRC2 cells (10). These findings show that GLS1 inhibition compromises de novo pyrimidine biosynthesis selectively in *VHL*<sup>-/-</sup> cells because it decreases the production of aspartate from glutamine carbons.

*VHL*<sup>+/+</sup> RCC cells adapt to GLS1 inhibition by stimulating glucose oxidation in the TCA cycle. To investigate the metabolic mechanism by which *VHL*<sup>+/+</sup> RCC cells can tolerate GLS1 inhibition, we labeled the pair of UMRC2 cells with [U-<sup>13</sup>C]<sub>6</sub>glucose and measured the <sup>13</sup>C enrichment of TCA cycle intermediates by GC-MS, with and without BPTES. The BPTES treatment increased the enrichment of M2 and M3 intermediates in the TCA cycle intermediates in *VHL*<sup>+/+</sup> but not in *VHL*<sup>-/-</sup> UMRC2 cells (Figure 2, E-G), showing that GLS1 inhibition stimulates glucose oxidation in the TCA cycle. The level of glucose oxidation in BPTES-treated *VHL*<sup>-/-</sup> UMRC2 cells was, in most cases, lower than or similar to that observed in BPTES-untreated *VHL*<sup>-/-</sup> cells (in particular for M2 enrichments). These observations are not a cell line-specific phenomenon; they were corroborated in the independent isogenic pair of *VHL*<sup>-/-</sup> and *VHL*<sup>+/+</sup> UMRC3 cells (Supplemental Figure 4), indicating that the activation of glucose oxidation reflects an adaptive metabolic response to GLS1 inhibition. Taken together these observations strongly suggest that GLS1 inhibition leads to glutamine-derived depletion of aspartate carbons in *VHL*<sup>+/+</sup> cells, which can be compensated by increased glucose oxidation. In contrast, *VHL*<sup>-/-</sup> cells lack these compensatory mechanisms and GLS1 inhibition results in depletion of pyrimidine intermediates.

*Inhibition of GLS1 selectively enhances intracellular ROS level through GSH biosynthesis repression.* In addition to being a source for de novo nucleoside synthesis, glutamine carbons are utilized for GSH biosynthesis. GSH is synthesized through the conjugation of cysteine, glycine, and glutamate, which is generated from glutamine by GLS1, and contributes to redox homeostasis (35). We hypothesized that glutamine deprivation would impair GSH biosynthesis and enhance intracellular ROS. To test this hypothesis, we cultured isogenic *VHL*<sup>-/-</sup> and *VHL*<sup>+/+</sup> UMRC2 cells with BPTES for 24 hours and measured the intracellular ROS levels by

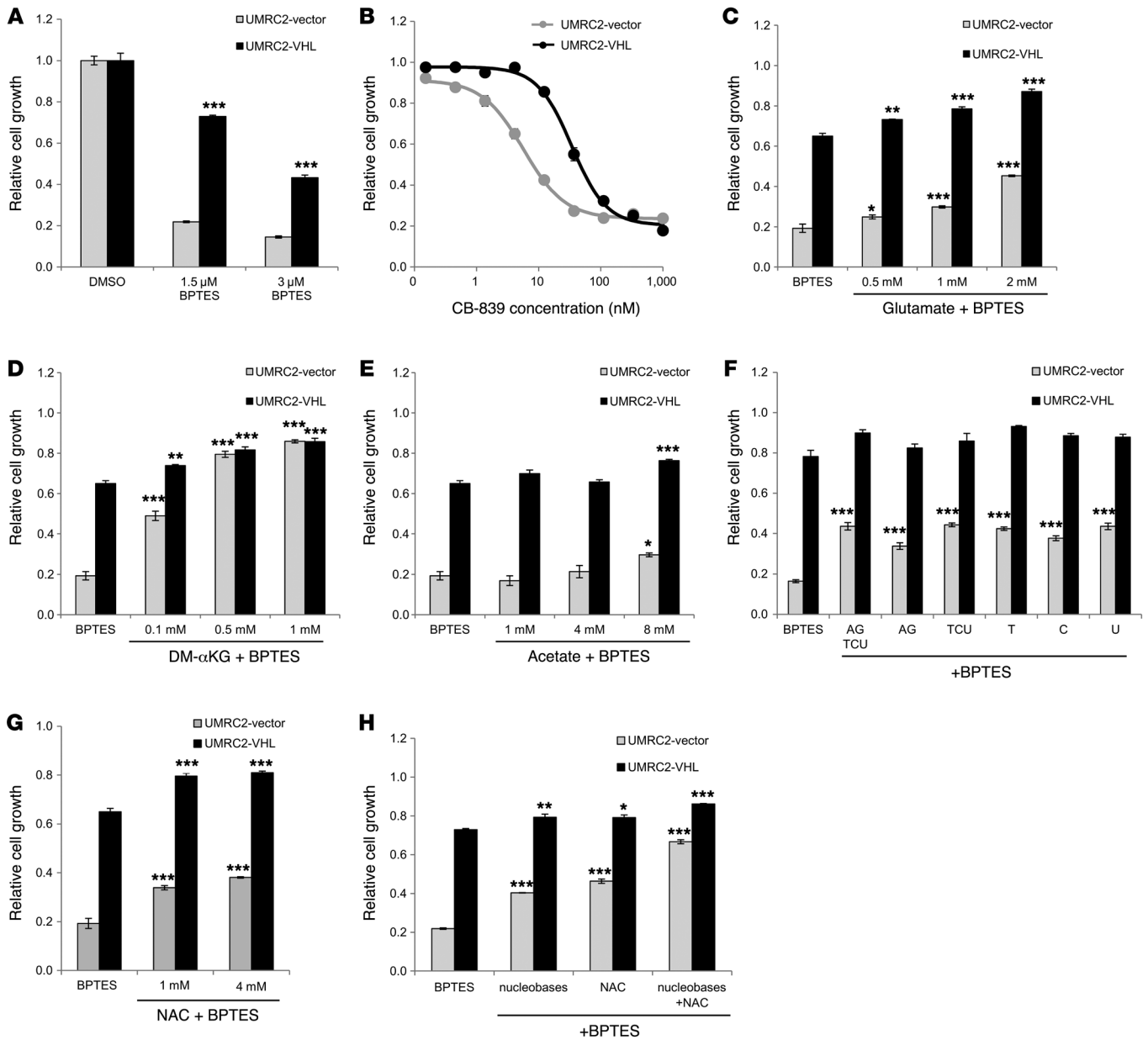


**Figure 4. Inhibition of GLS1 selectively impairs the growth of *VHL*<sup>-/-</sup> RCC cells, and exogenous metabolites rescue the growth inhibition effects.**

Isogenic pairs of *VHL*<sup>-/-</sup> and *VHL*<sup>+/-</sup> cells were cultured in DMSO or BPTES-containing medium for 72 hours, and cell growth was determined by crystal violet staining. Cell growth was normalized to the corresponding cell type (*VHL*<sup>-/-</sup> or *VHL*<sup>+/-</sup>) grown in DMSO-containing medium. (A and B) Effect of GLS1 inhibitor BPTES (A) and CB-839 (B) on the isogenic *VHL*<sup>-/-</sup> and *VHL*<sup>+/-</sup> UMR2C. (C–H) Cells were cultured in DMSO or 1.5  $\mu$ M BPTES-containing medium with supplementation of glutamate (C), DM- $\alpha$ KG (D), acetate (E), nucleobases (5  $\mu$ M) (F), NAC (G) or a combination of nucleobases (5  $\mu$ M) and NAC (4 mM) for 72 hours. Error bars represent SEM ( $n = 3$ ). \* $P < 0.05$ , \*\* $P < 0.01$ , \*\*\* $P < 0.001$ , Student's *t* test between *VHL*<sup>-/-</sup> and *VHL*<sup>+/-</sup> cells (A) and Dunnett's test against corresponding control conditions (C–H). A, adenine; G, guanine; T, thymine; C, cytosine; U, uracil.

2',7'-dichlorofluorescein diacetate (DCFDA) staining. GLS1 inhibition by BPTES increased DCFDA intensity dose-dependently, and the effect was more pronounced in *VHL*<sup>-/-</sup> UMR2 cells (Figure 3A). Notably, *VHL*<sup>-/-</sup> UMR2 cells had higher DCFDA intensity at the basal level, which suggests that *VHL*<sup>-/-</sup> cells are in more oxidative stress compared with *VHL*<sup>+/-</sup> cells. Addition of exogenous dimethyl  $\alpha$ KG (DM- $\alpha$ KG) and an antioxidant, *N*-acetylcysteine (NAC), rescued the increase of intracellular ROS level (Figure 3B). To investigate whether the ROS enhancement by GLS1 inhi-

bition was due to an impaired GSH biosynthesis, we measured the ratio of reduced to oxidized glutathione (GSH/GSSG ratio) after BPTES treatment for 24 hours. The BPTES treatment significantly decreased the GSH/GSSG ratios in a dose-dependent manner and selectively in *VHL*<sup>-/-</sup> UMR2 cells, showing that repression of biosynthesis by GLS1 inhibition plays a critical role in the elevation of intracellular ROS level (Figure 3C). Lastly, we evaluated synergistic effects of BPTES with a small molecular ROS enhancer, BRD56491, which can enhance intracellular ROS

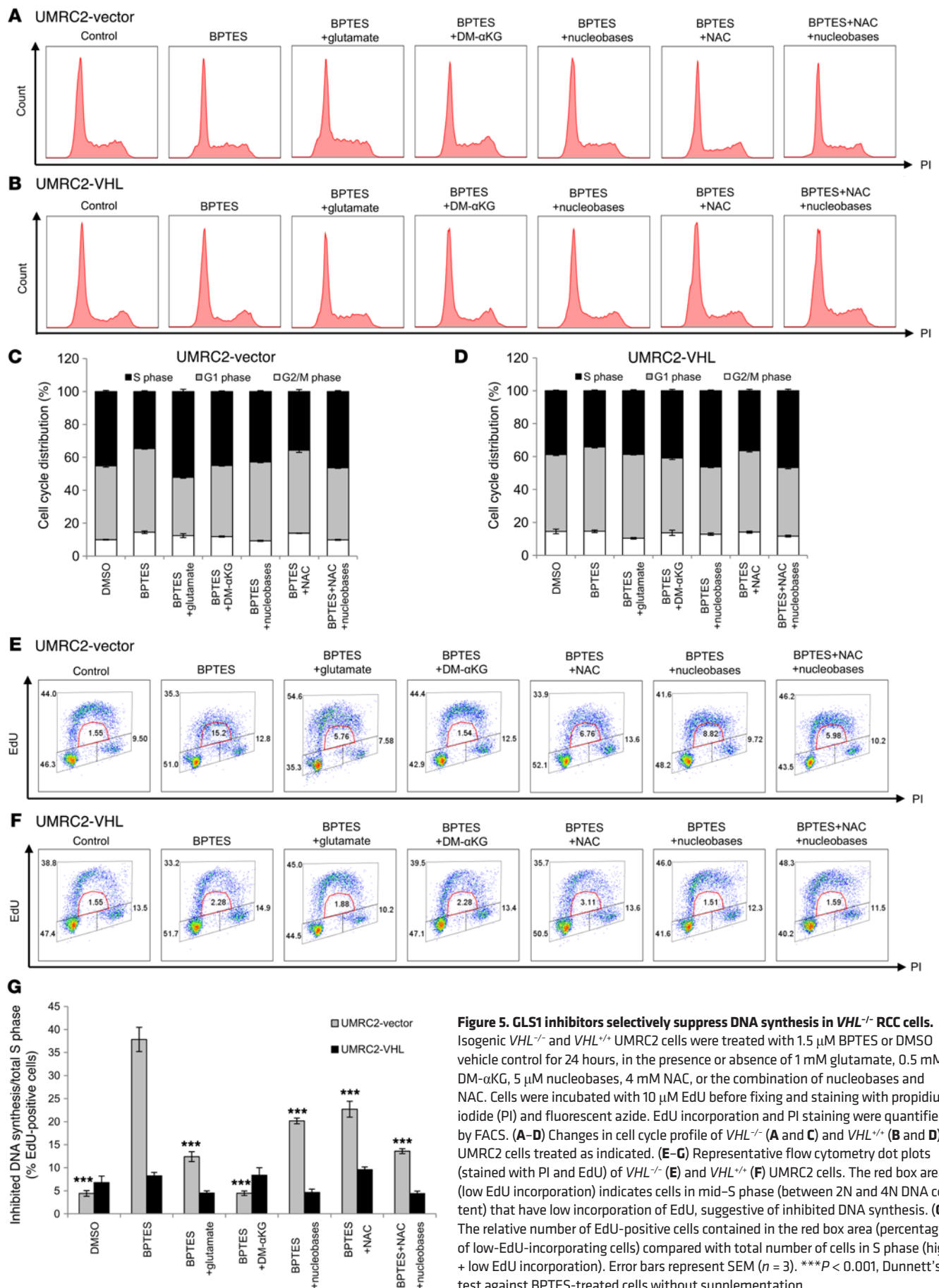


**Figure 5. GLS1 inhibitors selectively suppress DNA synthesis in *VHL*<sup>-/-</sup> RCC cells.** Isogenic *VHL*<sup>-/-</sup> and *VHL*<sup>+/+</sup> UMRC2 cells were treated with 1.5  $\mu$ M BPTES or DMSO vehicle control for 24 hours, in the presence or absence of 1 mM glutamate, 0.5 mM DM- $\alpha$ KG, 5  $\mu$ M nucleobases, 4 mM NAC, or the combination of nucleobases and NAC. Cells were incubated with 10  $\mu$ M EdU before fixing and staining with propidium iodide (PI) and fluorescent azide. EdU incorporation and PI staining were quantified by FACS. (A–D) Changes in cell cycle profile of *VHL*<sup>-/-</sup> (A and C) and *VHL*<sup>+/+</sup> (B and D) UMRC2 cells treated as indicated. (E–G) Representative flow cytometry dot plots (stained with PI and EdU) of *VHL*<sup>-/-</sup> (E) and *VHL*<sup>+/+</sup> (F) UMRC2 cells. The red box area (low EdU incorporation) indicates cells in mid-S phase (between 2N and 4N DNA content) that have low incorporation of EdU, suggestive of inhibited DNA synthesis. (G) The relative number of EdU-positive cells contained in the red box area (percentage of low-EdU-incorporating cells) compared with total number of cells in S phase (high + low EdU incorporation). Error bars represent SEM ( $n = 3$ ). \*\*\* $P < 0.001$ , Dunnett’s test against BPTES-treated cells without supplementation.

levels and synergistically induce cell death by combination with buthionine sulfoximine (BSO), an inhibitor of GSH biosynthesis (36). We cultured isogenic *VHL*<sup>-/-</sup> and *VHL*<sup>+/+</sup> UMRC2 cells in the presence of BPTES, BRD56491, or their combination and measured the intracellular ROS level. The combination of BPTES and BRD56491 synergistically enhanced the intracellular ROS level selectively in *VHL*<sup>-/-</sup> UMRC2 cells (Figure 3D), and selectively impaired the growth of *VHL*<sup>-/-</sup> UMRC2 cells (Supplemental Figure 5), which indicates that BPTES worked as an inhibitor of GSH biosynthesis similarly to BSO. These findings strongly support the hypothesis that GLS1 inhibition impairs GSH biosynthesis and enhances intracellular ROS level.

*Inhibition of GLS1 selectively impairs the growth of VHL-deficient human RCC cells.* The observations presented above raise the hypothesis that the compromised de novo pyrimidine synthesis and induction of ROS might be the mechanisms that confer, at least in part, a significantly higher sensitivity of *VHL*<sup>-/-</sup> cells to GLS1 inhibition compared with their *VHL*<sup>+/+</sup> isogenic counterparts. To test this hypothesis and to confirm that these observations are not cell line specific, we first treated a panel of *VHL*-deficient human RCC cell lines (UMRC2, RCC4, and UOK102) and their *VHL*-replete counterparts with GLS1 inhibitors BPTES and CB-839 (ref. 37; Figure 4, A and B; and Supplemental Figure 6). We showed that lack of *VHL* confers increased sensitivity to GLS1 inhibition. Moreover, we showed that exogenous administration of DM- $\alpha$ KG restored the viability of *VHL*<sup>-/-</sup> cells to a level equal to the one of *VHL*<sup>+/+</sup> cells and protects both types of cells from GLS1 inhibitor-mediated growth suppression (Figure 4D and Supplemental Figure 7). DM- $\alpha$ KG can freely convert to glutamate and glutamine in the cell and therefore provide carbons to metabolic pathways requiring adequate levels of glutamine. Addition of exogenous glutamate to tissue culture medium improved the growth of *VHL*<sup>-/-</sup> cells treated with BPTES, but to a much lesser extent than DM- $\alpha$ KG did (Figure 4C). In contrast to both glutamate and DM- $\alpha$ KG, addition of acetate minimally protected *VHL*<sup>-/-</sup> cells from GLS1 inhibitor-mediated growth suppression, and only at higher concentrations (Figure 4E). Lastly, to address directly whether inhibition of de novo pyrimidine synthesis contributes to the cell growth inhibition, we showed that supplementing the tissue culture medium of BPTES-treated *VHL*<sup>-/-</sup> and *VHL*<sup>+/+</sup> RCC cells with either pyrimidine or purine nucleobases partially but significantly (approximately 3-fold increase) improved cell survival of *VHL*<sup>-/-</sup> cells (Figure 4F). Supplementation of NAC also partially improved cell survival of *VHL*<sup>-/-</sup> cells (Figure 4G). Moreover, the combination of nucleobases and NAC had an additive effect in rescuing the growth inhibition effect of BPTES (Figure 4H), revealing that inhibition of de novo pyrimidine synthesis and increase of ROS independently contributed to the inhibition of cell proliferation. These observations were not cell type specific (Supplemental Figure 7). These experiments provide strong evidence that the sensitivity of *VHL*<sup>-/-</sup> cells to GLS1 inhibitors is an “on-target” outcome and that compromised de novo pyrimidine synthesis and disruption of redox homeostasis contribute, at least in part, to the cell growth suppression induced by GLS1 inhibitors. Our data also suggest that there are likely more processes in addition to perturbed pyrimidine and GSH biosynthesis affected by GLS1 inhibition.

*Inhibition of GLS1 selectively induces DNA replication stress in VHL<sup>-/-</sup> human RCC cells.* Next, we investigated the mechanism(s) by which compromised pyrimidine synthesis and ROS enhancement might lead to *VHL*<sup>-/-</sup> cell growth suppression. We tested isogenic *VHL*<sup>-/-</sup> and *VHL*<sup>+/+</sup> UMRC2 cells for apoptosis and senescence after a 3-day treatment with increasing doses of GLS1 inhibitor BPTES or CB-839. We detected no evidence of either increased apoptosis or senescence within this time frame, despite significant suppression of cell growth (data not shown). These observations led us to hypothesize that treatment with GLS1 inhibitors activates a glutamine-related cell cycle checkpoint and/or that the overall cell cycle is lengthened as a consequence of GLS1 inhibition. We investigated these possibilities by analyzing the cell cycle distribution of cells (propidium iodide staining) and the rate of DNA synthesis (pulse labeling with 5-ethynyl-2'-deoxyuridine [EdU] and propidium iodide staining). We did not detect a drastic change in the cell cycle distribution of either *VHL*<sup>-/-</sup> or *VHL*<sup>+/+</sup> cells when treated with BPTES (Figure 5, A–D). However, we noted that BPTES modestly reduced the fraction of S-phase cells in the *VHL*<sup>-/-</sup> but not the *VHL*<sup>+/+</sup> cell population (Figure 5, A–D). This reduction in S phase was suppressed by supplementation of glutamate, DM- $\alpha$ KG, and nucleobases. Consistently, EdU pulse labeling showed that DNA synthesis was reduced in *VHL*<sup>-/-</sup> cells compared with the isogenic *VHL*<sup>+/+</sup> cells upon treatment with BPTES (Figure 5, E and F: compare high to low incorporation of EdU during S phase; percentage of low-incorporation cells compared with total cells in S phase is shown in Figure 5G). This low incorporation of EdU by *VHL*<sup>-/-</sup> cells treated with BPTES can be restored to levels comparable to those of *VHL*<sup>+/+</sup> cells by supplementation of the culture media with DM- $\alpha$ KG or glutamate, and partially by nucleobases or NAC, all metabolites that “rescued” the suppression of *VHL*<sup>-/-</sup> cell growth by BPTES (Figure 4). The combination of nucleobases and NAC additively rescued the effect. This phenomenon is not cell line specific (Supplemental Figure 8); it can be detected as early as 24 hours after application of GLS1 inhibitor, and it lasts up to at least 72 hours (Supplemental Figure 9). This pattern of low EdU incorporation in association with inhibited synthesis of pyrimidines, in the absence of a “classic” cell cycle arrest, is reminiscent of DNA replication stress due to low nucleotide levels, an association that has been described before (38).

Low nucleotide levels might significantly delay nucleotide incorporation into nascent DNA, which may lead to exposure of single-stranded DNA and activation of the *ataxia telangiectasia* and Rad3-related (ATR) kinase-mediated checkpoint (39). The replication checkpoint is known to inhibit firing of replication origins. To test whether treatment with GLS1 inhibitors BPTES and CB-839 results in activation of the replication checkpoint, we assayed *VHL*<sup>-/-</sup> and *VHL*<sup>+/+</sup> cells for phospho-CBK1 and phospho-RPA32. Treatment of cells with GLS1 inhibitors at doses inducing significant cell growth delay did not lead to detectable changes in phosphorylation of CBK1 and RPA32 (Supplemental Figure 10). Similar to our findings, previous studies have shown that low concentrations of hydroxyurea, an inhibitor of deoxyribonucleotide triphosphate (dNTP) synthesis, also significantly slow down replication forks without inducing robust CBK1/RPA32 phosphorylation (40). Treatment of the isogenic *VHL*<sup>-/-</sup> and *VHL*<sup>+/+</sup> UMRC2 cells with hydroxyurea induced S-phase arrest selectively in *VHL*<sup>-/-</sup> UMRC2 cells, and phosphorylation of CBK1 was observed at

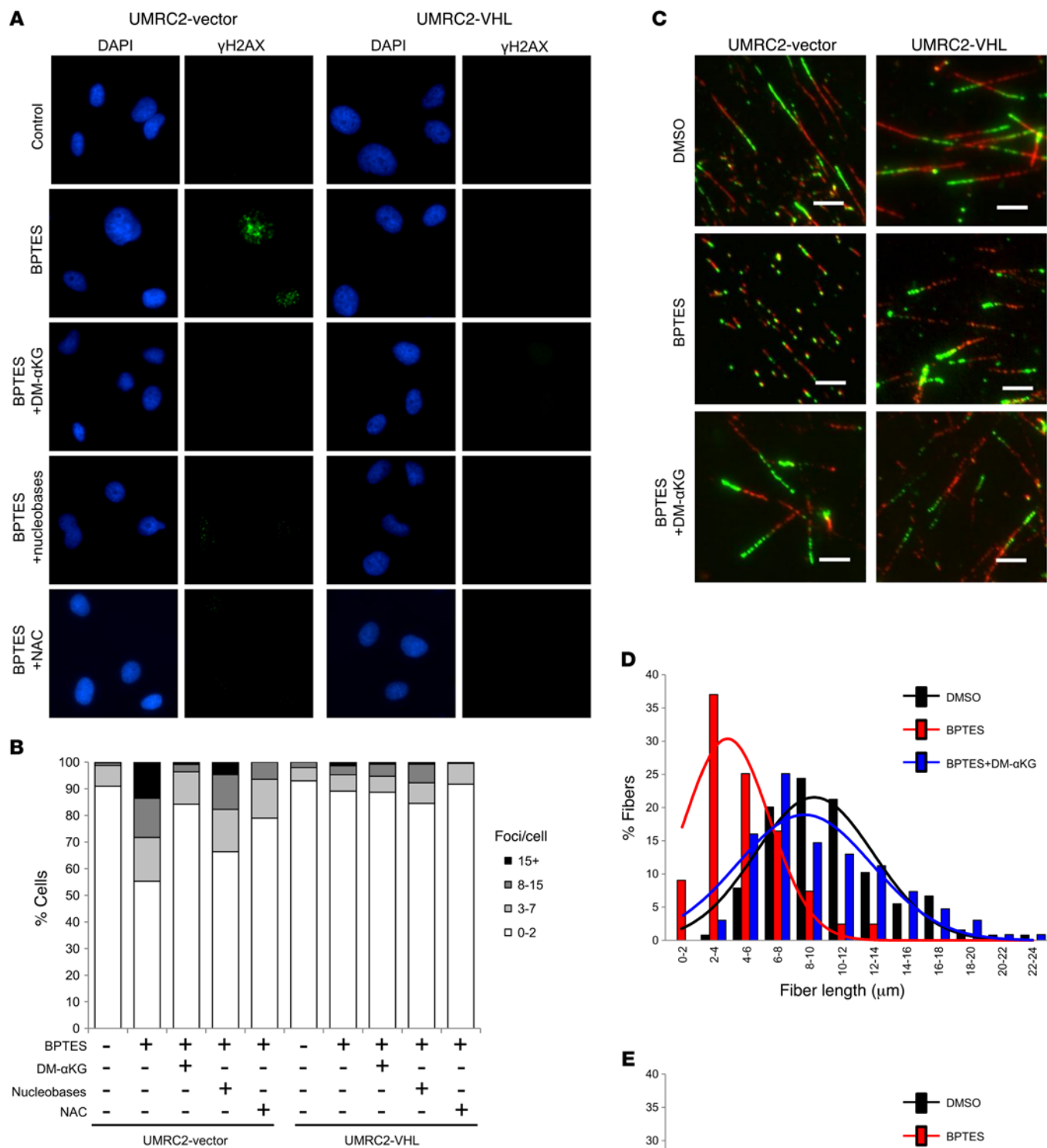


**Figure 6. GLS1 inhibitors selectively induce DNA replication stress in *VHL*<sup>-/-</sup> RCC cells.**

Isogenic *VHL*<sup>-/-</sup> and *VHL*<sup>+/+</sup> UMRC2 cells were treated with 1.5  $\mu$ M BPTES for 48 hours with or without supplementation with 0.5 mM DM- $\alpha$ KG, 5  $\mu$ M nucleobases, or 4 mM NAC. **(A)** DNA breaks were imaged by immunohistochemical detection of  $\gamma$ H2AX foci (green) and quantified. **(B)** Percentage of nuclei with the indicated number of  $\gamma$ H2AX foci. At least 100 nuclei for each condition were analyzed. **(C-E)** Detection and quantification of DNA replication stress by DNA fiber assay. Cells were treated with BPTES (1.5  $\mu$ M) or vehicle control in the presence or absence of DM- $\alpha$ KG (0.5 mM) and pulse-labeled with CldU (green) and IdU (red). **(C)** Representative images of DNA incorporation of CldU and IdU under different treatment conditions. Quantification of CldU and IdU incorporation in replication forks of *VHL*<sup>-/-</sup> **(D)** and *VHL*<sup>+/+</sup> **(E)** cells under different treatment conditions. At least 150 DNA fibers for each condition were analyzed.

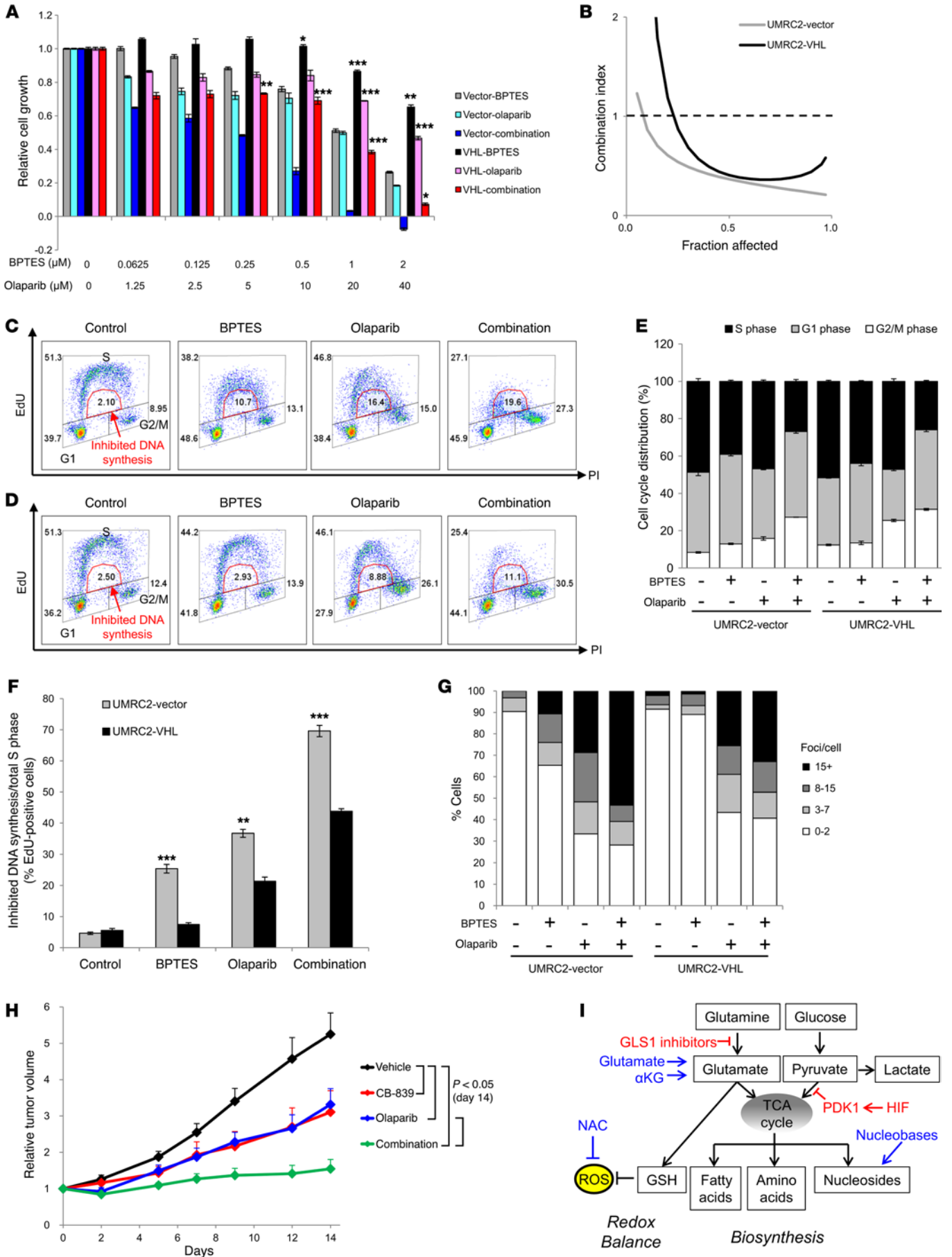


**Figure 7. PARP inhibition synergizes with GLS1 inhibitors to suppress the growth of *VHL*<sup>-/-</sup> RCC cells in vitro and in vivo.** (A) Isogenic *VHL*<sup>-/-</sup> and *VHL*<sup>+/+</sup> UMRC2 cells were cultured in the absence or presence of BPTES and the PARP inhibitor olaparib, at the indicated concentrations, for 72 hours. Cell growth was determined by crystal violet staining and normalized to the corresponding cell type (*VHL*<sup>-/-</sup> and *VHL*<sup>+/+</sup>) cultured in DMSO-containing medium. (B) Combination index values were determined using CompuSyn software. A combination index value less than 1 indicates drug synergy. (C–F) DNA synthesis rate of *VHL*<sup>-/-</sup> and *VHL*<sup>+/+</sup> UMRC2 cells, treated with 1.5 μM BPTES, 20 μM olaparib, or their combination, as quantified by EdU incorporation. Representative flow cytometry dot plots of *VHL*<sup>-/-</sup> (C) and *VHL*<sup>+/+</sup> (D) UMRC2 cells. (E) Cell cycle distributions of treated cells. (F) Percentage of low-EdU-incorporating cells (% cells in DNA replication stress) when treated with GLS1 inhibitor (BPTES), PARP inhibitor (olaparib), or their combination. (G) Percentage of nuclei with the indicated number of γH2AX foci after treatment of *VHL*<sup>-/-</sup> and *VHL*<sup>+/+</sup> UMRC2 cells with BPTES, olaparib, or their combination. At least 100 nuclei for each condition were analyzed. (H) Tumor growth of UMRC3 xenografts treated with vehicle control ( $n = 6$ ), CB-839 (200 mg/kg, twice daily,  $n = 7$ ), olaparib (75 mg/kg, once daily,  $n = 7$ ), or their combination ( $n = 8$ ). Error bars represent SEM. \* $P < 0.05$ , \*\* $P < 0.01$ , \*\*\* $P < 0.001$ , Student's  $t$  test between *VHL*<sup>-/-</sup> and *VHL*<sup>+/+</sup> UMRC2 cells.  $P$  values in A were corrected by Bonferroni method (to account for multiple comparisons). (I) Model diagram: HIF-1α/2α activates PDK1 and suppresses glucose and promotes glutamine utilization in the TCA cycle. Glutamate and TCA metabolites are required for biosynthesis and redox balance. GLS1 inhibitors selectively block biosynthesis and GSH production in HIF-expressing cells. Red labels inhibitory reactions. Blue labels metabolites/drug that can be administered to cells in order to bypass the effect of GLS1 inhibitors.

lower concentrations in *VHL*<sup>-/-</sup> cells compared with *VHL*<sup>+/+</sup> cells. Hydroxyurea selectively suppressed the growth of *VHL*<sup>-/-</sup> UMRC2 cells, suggesting that *VHL*-deficient cells are more susceptible to inhibition of nucleotide synthesis (Supplemental Figure 11). Our results suggest that GLS1 inhibitors suppress DNA synthesis but do not evoke the replication checkpoint strongly.

Compromised DNA synthesis could rise to double-stranded DNA breaks (DSBs) during replication, which are marked by γH2AX (40). To test whether GLS1 inhibition induces DSBs, we immunostained *VHL*<sup>-/-</sup> and *VHL*<sup>+/+</sup> UMRC2 cells for expression of γH2AX during treatment with GLS1 inhibitors in the presence or absence of metabolites that rescue BPTES-induced cell growth inhibition. A representative field is shown in Figure 6A. Quantification of γH2AX foci (Figure 6B) strongly suggests that *VHL*<sup>-/-</sup> but not *VHL*<sup>+/+</sup> cells undergo DNA replication stress upon treatment with GLS1 inhibitors, which, in turn, can be mitigated by addition of DM-αKG, nucleobases, or NAC (Figure 6, A and B). Cotreatment of BPTES and BRD56491, the small-molecule ROS enhancer, synergistically induced DNA replication stress quantified by EdU incorporation and γH2AX, supporting the hypothesis that increase of ROS plays a key role in inducing DNA damage (Supplemental Figure 12). To corroborate this observation that GLS1 inhibition induces DNA replication stress with an independent assay, we performed a DNA fiber assay that directly quantifies the origins and speed of DNA replication forks. Isogenic *VHL*<sup>-/-</sup> and *VHL*<sup>+/+</sup> cells, treated with BPTES or vehicle control in the presence or absence of DM-αKG, were labeled sequentially with 5-Chloro-2'-deoxyuridine (CldU) and 5-Iodo-2'-deoxyuridine (IdU) nucleosides. Nucleoside incorporation was imaged by nucleoside-specific antibodies (Figure 6C), and the length of labeled nucleoside fibers was quantified (Figure 6, D and E). Treatment of *VHL*<sup>-/-</sup> but not *VHL*<sup>+/+</sup> UMRC2 cells with BPT-

ES significantly reduced progression of DNA replication forks (Figure 6D), a phenomenon totally reversed by addition of DM-αKG (Figure 6, C and D). Taken together these data strongly support the model whereby treatment of *VHL*<sup>-/-</sup> cells with GLS1 inhibitors compromises the synthesis of pyrimidines and induces oxidative stress, leading to a significant DNA replication stress and growth arrest.

*PARP inhibitors synergize with GLS1 inhibitors in enhancing DNA replication stress and cell growth arrest of *VHL*<sup>-/-</sup> human RCC cells.* Exploiting DNA replication stress of cancer cells has been emerging as an attractive strategy for targeted therapy (41). We therefore tested whether the DNA replication stress selectively induced in *VHL*<sup>-/-</sup> cells by GLS1 inhibitors could be enhanced by further interference with DNA synthesis, DNA damage, or DNA repair mechanisms. We treated *VHL*<sup>-/-</sup> and *VHL*<sup>+/+</sup> RCC cells with BPTES alone or in combination with hydroxyurea, 5-fluorouracil, or the orotate dehydrogenase inhibitor teriflunomide (all agents that inhibit DNA synthesis by interfering with nucleotide biogenesis or their incorporation into DNA) and showed no synergistic effect between these drugs and GLS1 inhibitors with regard to cell growth suppression (data not shown). In addition, treatment of cells with increasing doses of the DNA chemotherapeutic agent cis-platinum in combination with BPTES resulted in an additive but not synergistic effect with regard to growth suppression (data not shown). In contrast, when we combined a PARP inhibitor, olaparib, with the GLS1 inhibitor BPTES or CB-839, we detected a synergistic effect between the 2 agents in cell growth inhibition (Figure 7A) as well as DNA replication stress quantified by EdU incorporation (Figure 7, C, D, and F) and γH2AX foci formation (Figure 7G). The cells in S phase were significantly decreased by the combination treatment (Figure 7E), suggesting that DNA synthesis was strongly suppressed by the combination. The synergistic effect (Figure 7B) was evaluated by the Chou-Talalay method (42). This synergism was detected in several cell lines and within a range of concentrations (Supplemental Figure 13), and in vivo in the xenograft model (Figure 7H and Supplemental Figure 14 and 16, and Supplemental Table 1). No significant body weight loss was detected in animals treated in the various arms (Supplemental Figure 14C), indicating that the combination treatment with CB-839 and olaparib was well tolerated in this preclinical setting.

We showed that HIF-1α/2α is necessary and sufficient for reprogramming cancer cell metabolism by *VHL* (10). To corroborate the link between HIF-1α/2α and sensitivity to CB-839 as a single agent and in combination with olaparib, we infected *VHL*-replete cells with the *VHL*-immune HIF-2α (P405A/P531A) mutant or empty vector as control and treated the derived cell lines with CB-839, olaparib, and their combination. Consistent with our previously published findings, we show that HIF-2α expression is sufficient to render *VHL*-replete cells sensitive to CB-839 as a single agent and in combination with olaparib (Supplemental Figure 15).

The work presented here provides, for the first time to our knowledge, an insight into one of putatively many mechanisms by which GLS1 inhibitors might compromise the growth of *VHL*-deficient human RCC cell lines, namely induction of DNA replication stress. The identification of such a mechanism led to a hypothesis-driven testing of the synergistic combination of PARP with GLS1 inhibitors for treatment of clear cell RCC tumors. This translational significance of these observations is direct and clinically testable.

## Discussion

In this study, by tracing the fate of glucose and glutamine in central carbon metabolism, we showed that loss of *VHL* redirects glutamine carbons for pyrimidine biosynthesis in RCC cells, via RC. Inhibition of GLS1 decreased the levels of aspartate and pyrimidine intermediates preferentially in *VHL*<sup>-/-</sup> cells, suggesting that glutamine-derived aspartate is required to maintain pyrimidine biosynthesis in RCC cells. We also showed that GLS1 inhibition increased intracellular ROS through repression of GSH biosynthesis. Inhibition of GLS1 results in suppression of de novo pyrimidine synthesis and induction of oxidative stress, leading to DNA replication stress of *VHL*<sup>-/-</sup> cells and growth arrest. Finally, we showed that the biological effect of GLS1 inhibitors can be significantly enhanced by the administration of PARP inhibitors in vitro and in vivo. These observations provide mechanistic insights into the metabolic reprogramming of *VHL*<sup>-/-</sup> RCC cells and highlight novel strategies for treatment of *VHL*-deficient tumors.

Our current studies do not delineate the putative role of the pentose phosphate pathway (PPP), through production of 5-phosphoribosyl-phosphate, in the de novo synthesis of purine and pyrimidine nucleotides. HIF-1 $\alpha$ /2 $\alpha$  appears to reduce activity of oxidative PPP, but, in contrast, it induces the expression of transketolase, thereby likely maintaining the levels of ribose 5-phosphate through the nonoxidative arm of PPP (43). In our RCC cell lines, we did not observe significant changes in the oxidative PPP activity, as determined using the [1,2-<sup>13</sup>C<sub>2</sub>]glucose tracer (data not shown). Here we assessed the effect of BPTES at the level of N-carbamoyl-aspartate and N-carbamoyl-phosphate, which lie upstream of the condensation of 5-phosphoribosyl-phosphate with orotate. Further experiments are necessary to test the putative role of HIF-1 $\alpha$ /2 $\alpha$  in regulating PPP and the effect of GLS1 inhibition on the contribution of PPP to the de novo pathway of pyrimidine biosynthesis in RCC cells.

In this study we showed that *VHL*<sup>-/-</sup> cells had a higher intracellular ROS level compared with *VHL*<sup>+/+</sup> cells (Figure 3). In other words, *VHL*<sup>-/-</sup> cells are in more oxidative stress at the basal level. HIF transcriptional factors are known to activate NADPH oxidases of the NOX family (44), which are one of the major sources of ROS, and the activation of the NADPH oxidases by HIF in *VHL*<sup>-/-</sup> cells could be one of the mechanisms of oxidative stress. *VHL*<sup>+/+</sup> cells had a higher DNA synthesis rate than *VHL*<sup>-/-</sup> cells (Figure 6, D and E). DNA synthesis rates in DMSO control *VHL*<sup>-/-</sup> and *VHL*<sup>+/+</sup> cells were 10.3  $\pm$  3.7  $\mu$ m/40 min ( $n$  = 254) and 11.5  $\pm$  3.4  $\mu$ m/40 min ( $n$  = 235), respectively ( $P$  < 0.001), suggesting that DNA synthesis in *VHL*<sup>-/-</sup> cells is partially inhibited at the basal level owing to the oxidative stress.

Our current work provides insights into the mechanism by which restriction of glutamine carbons leads to cell growth inhibition. We showed that *VHL*<sup>-/-</sup> cells undergo DNA replication stress when treated with GLS1 inhibitors, which is consistent with the report from Dang's group that showed blockade of DNA replication by GLS1 inhibition in MYC-dependent human B cell lymphoma (45). The induction of DNA replication stress upon GLS1 inhibition probably represents a broader paradigm in which glutamine addiction at large, induced by different oncogenic mechanisms (such as HIF expression, MYC amplification, K-Ras mutation, tumor-related hypoxia, or other oncogenic mechanisms), renders cells sensitive to GLS1 inhibition as a single agent and/or in combination with olaparib.

Pyrimidine nucleotide availability and oxidative stress appear to be involved, at least in part, in the generation of replication stress, since supplementation of nucleobases or NAC to the tissue culture medium partially but significantly decreased DNA replication stress (as evidenced by EdU incorporation and  $\gamma$ H2AX staining), leading to a significant increase in cell proliferation. The non-complete restoration of cell growth by addition of nucleotides is very likely due to the fact that glutamine restriction results in additional biomass synthesis deficiencies not directly examined here, such as lipogenesis (7). Addition of a cell-permeable form of  $\alpha$ KG completely restored cell proliferation in *VHL*<sup>-/-</sup> UMRC2 cells, while addition of glutamate alleviated replication stress and supported cell proliferation to a lesser extent than  $\alpha$ KG. These differences could be attributed to different rates of cell incorporation of a specific metabolite; for example, the rate of receptor-mediated glutamate uptake may be different from that of the cell-permeable form of  $\alpha$ KG. The fact that  $\alpha$ KG and glutamate can contribute to biosynthesis of both pyrimidine and GSH would explain the mechanisms by which DM- $\alpha$ KG almost completely rescued cell growth and DNA replication stress. Alternatively these differences in metabolite capacity to restore glutamine-dependent cell growth may be linked to the pleiotropic functions of the metabolite; for example,  $\alpha$ KG, in addition to substituting in the TCA cycle for glutamine carbons, is likely to activate an epigenetic DNA methylation program that affects cell proliferative state (46).

Specific oncogenic events have been shown to regulate nucleotide pools directly or indirectly. Cell transformation by HPV oncoproteins E6/E7 or exogenous cyclin E led to decreased nucleotide levels and DNA replication stress, likely as an outcome of enhanced utilization of nucleosides in increased DNA synthesis (38). Ben-Sahra et al. reported that mTORC1-activated protein S6 kinase 1 directly phosphorylates S1859 on CAD (carbamoyl-phosphate synthetase 2, aspartate transcarbamoylase, dihydroorotase), the enzyme that catalyzes the first 3 steps of de novo pyrimidine synthesis in order to support TORC1-mediated anabolic processes (47). Loss of PKM2 inhibits purine production and the ability of cells to synthesize DNA and progress through the cell cycle; the exact mechanism of this phenomenon is currently under investigation (48). Our data suggest that loss of *VHL* impacts on pyrimidine production, at least in part, through reprogramming of cells to utilize glutamine carbons for aspartate synthesis.

Recently, it has been shown that primary and metastatic mouse orthotopic brain tumors have the capacity to simultaneously oxidize acetate and glucose but not glutamine, in vivo (49). Supplementation of *VHL*<sup>-/-</sup> cells with acetate did not mitigate the growth-suppressive effect of GLS1 inhibitors in vitro (Figure 4E). This observation, although made in vitro, indicates that substrate preference of cancer cells may be tissue specific or may depend on the molecular fabric of the specific cancers, as has already been suggested by in vivo metabolic labeling experiments (50). Our data strongly support the notion that *VHL*-deficient RCC cells heavily rely on glutamine for anabolic reactions. The Cancer Genome Atlas analysis of clear cell RCC tumors suggests a significant correlation between a worsened prognosis and increased glutamine transporters, suggesting that avid glutamine metabolism might be a metabolic marker of RCC (51).

Understanding the mechanism(s) by which GLS1 inhibitors induce cell growth arrest in *VHL*<sup>-/-</sup> RCC cells provides major opportunities for combination therapies that will synergize with GLS1 inhibitors in treating RCC and hypoxia-driven tumors. Recently, GLS1 inhibitor BPTES or CB-839 was reported to synergize with HSP90 inhibition in mTORC1-driven tumor cells (35),  $\beta$ -lapachone in pancreatic cancer (52), or BCL-2 inhibition in acute myeloid leukemia (53). Here we show that PARP inhibitors exert a synergistic effect in cell growth suppression when combined with GLS1 inhibitors. PARP1 and PARP2 promote the repair of DNA damage by a base excision repair mechanism and contribute to the restarting of replication forks that arrested at damaged sites. It is therefore not surprising that PARP inhibitors have attracted major interest as drugs that may target tumors with defective DNA damage response pathways, such as tumors with germline or somatic inactivation of *BRCA1/2* (54, 55). Indeed, Juvekar et al. showed that PARP inhibitors synergize with PI3K inhibitors for the treatment of *BRCA1*<sup>-/-</sup>-driven breast cancers (56). PARP inhibitors are currently being tested in numerous late-stage clinical trials targeting tumors characterized by deficiency in DNA damage response pathways, and they are FDA approved for treatment of *BRCA1/2*<sup>-/-</sup> advanced ovarian cancer (57).

The importance of the work presented here consists in providing a novel mechanism for inhibition of *VHL*<sup>-/-</sup> cell growth by GLS1 inhibition (DNA replication stress) and, based on this mechanism, the clinically testable hypothesis that GLS1 inhibitors can synergize with PARP inhibitors for treatment of renal cancer and possibly cancers with defects in DNA repair pathways.

## Methods

**Cell culture and metabolic labeling.** All cell lines were obtained from ATCC, tested for mycoplasma, cultured in 5% CO<sub>2</sub> incubators, and maintained in DMEM (GIBCO BRL) containing 10% FBS (Hyclone) supplemented with penicillin-streptomycin (Invitrogen). The pairs of *VHL*-deficient/*VHL*-replete UMRC2, UMRC3, RCC4, and UOK102 cell lines were generated as described previously (10). Isotopic labeling experiments were conducted as described previously (10), with the following modifications. In brief, cells were seeded in either 6-well plates (for GC-MS analyses) or 10-cm plates (for LC-MS/MS analyses) and cultured with glucose- and glutamine-free DMEM (basal DMEM; Sigma-Aldrich, D5030) containing 10% dialyzed FBS (Hyclone), supplemented with 10 mM glucose and 2 mM glutamine. We confirmed that these concentrations do not affect the growth rate of our cell lines (data not shown) and better reflect physiological conditions. [U-<sup>13</sup>C<sub>6</sub>]glutamine, [1-<sup>13</sup>C<sub>5</sub>]glutamine, and [U-<sup>13</sup>C<sub>6</sub>]glucose were obtained from Cambridge Isotope Labs. Metabolic labeling of polar metabolites with the appropriate tracer was conducted for either 24 or 48 hours, as indicated.

**Metabolic extractions and GC-MS and LC-MS/MS analysis.** For GC-MS analyses, metabolic activity was quenched with 400  $\mu$ l (-80°C) methanol, and 400  $\mu$ l distilled H<sub>2</sub>O was added after 1 minute. Cellular extracts were immediately collected in tubes by pipette-scraping of the wells. Two volumes (800  $\mu$ l) of (-20°C) chloroform were added to each tube, and extracts were vortexed for 15 seconds and centrifuged at 12,000 g for 10 minutes at 4°C. The aqueous phase containing amino and organic acids was evaporated using a vacuum centrifuge at 4°C. The dried metabolites were reacted with 30  $\mu$ l of 2% methoxyamine hydrochloride in pyridine (MOX reagent, Thermo Fisher Scientific)

for 1.5 hours at 37°C, derivatized by addition of 45  $\mu$ l of *N*-methyl-*N*-(*tert*-butyldimethylsilyl) trifluoroacetamide plus 1% *tert*-butyldimethylchlorosilane (MBTSTFA + 1% TBDMCS), and subjected to GC-MS analysis, as described previously (7). For LC-MS/MS analyses, the medium was aspirated and the plates rinsed with PBS. Metabolic quenching was achieved using a methanol/H<sub>2</sub>O solution (0.8:0.2) at -80°C, and plates were put in the -80°C freezer for 15 minutes. Subsequently, cellular extracts were collected in tubes by scraping of the plates in dry ice, and centrifuged at 12,000 g for 10 minutes at 4°C. The supernatant containing the metabolic extract was transferred into clean tubes, evaporated using a vacuum centrifuge at 4°C, and dissolved in 20  $\mu$ l distilled H<sub>2</sub>O. The metabolic extracts were subjected to LC-MS/MS analyses as described previously (58).

**DNA extraction and GC-MS analysis.** At the conclusion of the labeling period, cells were detached by trypsinization and centrifuged at 150 g for 5 minutes. The supernatant was aspirated and the DNA isolated from the cell pellet using a DNeasy Blood & Tissue column (Qiagen). Column elution was performed with 100  $\mu$ l of DNase-free water and the DNA concentration determined using a Nanodrop instrument (Thermo Fisher Scientific, catalog 9836718). To hydrolyze the DNA into individual free bases, 200  $\mu$ l of 88% formic acid was added to the DNA-containing tubes, and the solution (formic acid/H<sub>2</sub>O, 2:1) transferred to vacuum hydrolysis tubes (Thermo Fisher Scientific) for hydrolysis at 140°C for 1 hour. Optimization experiments showed that no significant gain of GC-MS signal was obtained by extending of the hydrolysis time. The hydrolyzed DNA was evaporated under air flow. Similarly to the polar metabolites, the free bases were derivatized using the MOX reagent and MBTSTFA + 1% TBDMCS, as previously described for the GC-MS analysis of nucleotide bases (58). The derivatization volume was adjusted so as to obtain a final DNA concentration of either 50 ng/ $\mu$ l or 100 ng/ $\mu$ l, based on the Nanodrop quantification. For the GC-MS analysis, either 1  $\mu$ l (of 100 ng/ $\mu$ l) or 2  $\mu$ l (of 50 ng/ $\mu$ l) sample was injected in splitless mode. The GC-MS parameters were as previously described for polar metabolites (7); the GC oven temperature ramp was slightly modified to allow a better separation of late-elution free bases, in particular, adenine and guanine.

**Intracellular ROS level and GSH/GSSG ratio measurement.** Intracellular ROS level was determined by staining of the cells with carboxy-DCFDA (Invitrogen, catalog C369). Cells were washed with PBS and incubated with 5  $\mu$ M carboxy-DCFDA for 10 minutes at 37°C. The cells were processed and analyzed using a BD LSRII Flow Cytometer System (BD Biosciences) and FlowJo software (Tree Star). GSH/GSSG ratio was determined using GSH/GSSG-Glo (Promega, catalog V6611) according to the manufacturer's protocol.

**Relative cell growth.** Cells were cultured in basal DMEM supplemented with 10 mM glucose, 2 mM glutamine, and 10% dialyzed FBS. Cells were cultured in 24-well plates over 3 days with drugs, until confluence was reached in the DMSO-treated control wells. Relative cell growth was assayed by crystal violet staining. In brief, the medium was aspirated, and cells were fixed with a 6.25% glutaraldehyde solution for 10 minutes. The fixating solution was aspirated and the wells rinsed twice with distilled H<sub>2</sub>O, stained with a 0.1% crystal violet solution for 30 minutes, and thoroughly rinsed with H<sub>2</sub>O. The cells were stained on the day of treatment (day 1) and after 3 days of incubation with drugs (day 4). Crystal violet was extracted with 10% acetic acid, and the absorbance (Abs) at 590 nm was measured. Relative cell growth was calculated according to the following equations:

When  $\text{Abs}_{\text{drug,day4}} \geq \text{Abs}_{\text{day1}}$ , relative cell growth =  $(\text{Abs}_{\text{drug,day4}} - \text{Abs}_{\text{day1}}) / (\text{Abs}_{\text{DMSO,day4}} - \text{Abs}_{\text{day1}})$ . When  $\text{Abs}_{\text{drug,day4}} < \text{Abs}_{\text{day1}}$ , relative cell growth =  $(\text{Abs}_{\text{drug,day4}} - \text{Abs}_{\text{day1}}) / \text{Abs}_{\text{day1}}$ . Negative relative cell growth values mean that the cells were killed by the drugs. For the evaluation of synergistic effect of 2 drugs, combination index values were determined by the Chou-Talalay method using CompuSyn (ComboSyn) software. A combination index value less than 1 indicates drug synergy.

**Cell cycle and EdU incorporation.** EdU incorporation and DNA content were analyzed by flow cytometry 30 minutes before cell collection, EdU was added to the culture medium at a concentration of 10  $\mu\text{M}$ , and the cells were trypsinized and fixed with 75% ethanol. The cells were stained with the Click-it EdU Flow Cytometry Assay Kit (Invitrogen) and propidium iodide with RNase according to the manufacturer's protocol. The cells were processed and analyzed using a BD LSRII Flow Cytometer System (BD Biosciences) and FlowJo software (Tree Star).

**Immunofluorescence for detection of  $\gamma\text{H2AX}$  foci.** Cells were fixed in 3.7% formaldehyde/PBS for 10 minutes, permeabilized with 0.5% Triton/PBS for 10 minutes, and blocked with 1% BSA/PBS for 30 minutes. The cells were incubated for 2 hours with anti- $\gamma\text{H2AX}$  (clone D17A3, 1:400; Cell Signaling Technology; catalog 76315), followed by 1% BSA/PBS wash and then Alexa Fluor 488-goat anti-rabbit IgG secondary antibody (1:200; Molecular Probes, Thermo Fisher Scientific; catalog A-11008) for 1 hour, and counterstained with DAPI. Fluorescent images were taken with EVOS FL Auto Cell Imaging System (Life Technologies). Foci were counted using ImageJ software (NIH), and at least 100 nuclei for each condition were analyzed.

**DNA fiber assay.** Cells were labeled with CldU (100  $\mu\text{M}$ ) for 20 minutes, washed, and labeled with IdU (250  $\mu\text{M}$ ) for 20 minutes. DNA fibers were spread as described (59). Briefly, 2.5  $\mu\text{l}$  of the cells suspended in PBS ( $\sim 10^6$  cells/ml) was spotted onto a glass slide and allowed to briefly dry; 7.5  $\mu\text{l}$  of spreading buffer (0.5% SDS, 200 mM Tris-HCl pH 7.4, 50 mM EDTA) was dropped on the dried cells and incubated for 10 minutes. Slides were tilted ( $\sim 15^\circ$ ) to allow lysed cell mixture to slowly run down the slide. The spread DNA was air-dried, fixed in cold methanol/acetic acid (3:1) for 3 minutes, and stored at  $4^\circ\text{C}$  overnight. Fibers were denatured in 2.5 M HCl for 30 minutes and blocked with 2% BSA/0.05% Tween for 1 hour at  $37^\circ\text{C}$ . Detection of CldU and IdU tracts was carried out using rat anti-BrdU (AbD Serotec, OBT0030) (1:50) and mouse anti-BrdU (BD Biosciences, 347580) (1:40) for 1 hour at  $37^\circ\text{C}$ , followed by Alexa Fluor 488-anti-mouse (1:100) and Cy3-anti-rat (Jackson ImmunoResearch) (1:100) for 30 minutes at  $37^\circ\text{C}$ . Slides were washed in PBS and mounted using VectaShield (Vector Laboratories). Fibers were imaged at  $\times 60$  magnification with a Nikon 90i.

**Immunoblots and antibodies.** Cells were rinsed with ice-cold PBS. Cell lysates were obtained by addition of RIPA buffer containing pro-

tease inhibitors, and incubation was performed for 30 minutes at  $4^\circ\text{C}$ . Subsequently, cell lysates were scraped and collected into tubes and clarified by centrifugation, and the proteins resolved in SDS-PAGE gels, transferred to PVDF membrane (Bio-Rad), and detected by immunoblotting using the following antibodies: anti-CHK1 (Santa Cruz Biotechnology Inc.; sc-8408), anti-CHK1-pS345 (Cell Signaling Technology; catalog 2341), anti-RPA32 (Thermo Fisher Scientific; PA5-22256), and anti-RPA32-pS33 (Bethyl Laboratories; A300-246A).

**Xenograft studies.** All protocols conformed to institutional regulations. UMRC3 cells were injected s.c. in nu/nu mice on the right flank ( $5 \times 10^6$  cells/injection). Once tumors reached an average volume of approximately 100–300  $\text{mm}^3$ , mice were randomized into 4 arms. Mice were treated by oral gavage with vehicle control, CB-839 (200 mg/kg, twice daily), olaparib (75 mg/kg, once daily), or the combination of CB-839 and olaparib. CB-839 was a gift of Calithera Biosciences Inc., and olaparib was a gift of AstraZeneca. Tumor grafts were measured with calipers, and tumor volumes were calculated as length  $\times$  width $^2 \times 0.5$ . The tumors were harvested and weighed at the experimental endpoint.

**Statistics.** Statistical significance was determined using 2-tailed Student's *t* test, Dunnett's test, or Tukey's test. A *P* value of less than 0.05 was considered statistically significant. Error bars represent the SEM, unless otherwise noted.

**Study approval.** Animal experiments were conducted according to a protocol reviewed and approved by the Massachusetts General Hospital Subcommittee on Research Animal Care—Office of Laboratory Animal Welfare Assurance A3596-01.

## Author contributions

AO, PAG, DC, LL, MS, and SAY conducted the experiments described in the paper. FC was responsible for immunohistochemistry of tumor xenografts. AO, PAG, ASR, RL, GS, LZ, and OI provided critical insights and/or conceived and designed the experiments. AO and OI wrote the manuscript. All authors reviewed the manuscript, agreed with results, and provided comments on the manuscript. OI supervised and coordinated the work.

## Acknowledgments

This work was supported by NIH grant NCI R01 CA160458 (to OI and GS) and an award from the Foundation for Research in Cell Biology Cancer and Cardiology (to OI).

Address correspondence to: Othon Iliopoulos, Center for Cancer Research at Massachusetts General Hospital Cancer Center and Harvard Medical School, 149 13th Street, Charlestown, Massachusetts 02129, USA. Phone: 617.724.3404; E-mail: oliopoulos@partners.org.

- Gatenby RA, Gillies RJ. Why do cancers have high aerobic glycolysis? *Nat Rev Cancer*. 2004;4(11):891–899.
- Masson N, Ratcliffe PJ. Hypoxia signaling pathways in cancer metabolism: the importance of co-selecting interconnected physiological pathways. *Cancer Metab*. 2014;2(1):3.
- Ebert BL, Gleadle JM, O'Rourke JF, Bartlett SM, Poulton J, Ratcliffe PJ. Isoenzyme-specific regulation of genes involved in energy metabolism by hypoxia: similarities with the regulation of erythropoietin. *Biochem J*. 1996;313(Pt 3):809–814.
- Kim JW, Tchernyshov I, Semenza GL, Dang CV. HIF-1-mediated expression of pyruvate dehydrogenase kinase: a metabolic switch required for cellular adaptation to hypoxia. *Cell Metab*. 2006;3(3):177–185.
- Papandreou I, Cairns RA, Fontana L, Lim AL, Denko NC. HIF-1 mediates adaptation to hypoxia by actively downregulating mitochondrial oxygen consumption. *Cell Metab*. 2006;3(3):187–197.
- Gordan JD, Bertout JA, Hu CJ, Diehl JA, Simon MC. HIF-2 $\alpha$  promotes hypoxic cell proliferation by enhancing c-myc transcriptional activity. *Cancer Cell*. 2007;11(4):335–347.
- Metallo CM, et al. Reductive glutamine metabolism by IDH1 mediates lipogenesis under hypoxia. *Nature*. 2011;481(7381):380–384.
- Mullen AR, et al. Reductive carboxylation supports growth in tumour cells with defective mitochondria. *Nature*. 2011;481(7381):385–388.
- Wise DR, et al. Hypoxia promotes isocitrate dehydrogenase-dependent carboxylation of  $\alpha$ -ketoglutarate to citrate to support cell growth and viability. *Proc Natl Acad Sci U S A*. 2011;108(49):19611–19616.

10. Gameiro PA, et al. In vivo HIF-mediated reductive carboxylation is regulated by citrate levels and sensitizes VHL-deficient cells to glutamine deprivation. *Cell Metab.* 2013;17(3):372–385.
11. Kaelin WG. The von Hippel-Lindau tumour suppressor protein: O<sub>2</sub> sensing and cancer. *Nat Rev Cancer.* 2008;8(11):865–873.
12. Hensley CT, Wasti AT, DeBerardinis RJ. Glutamine and cancer: cell biology, physiology, and clinical opportunities. *J Clin Invest.* 2013;123(9):3678–3684.
13. Tennant DA, Durán RV, Gottlieb E. Targeting metabolic transformation for cancer therapy. *Nat Rev Cancer.* 2010;10(4):267–277.
14. Dang CV. Links between metabolism and cancer. *Genes Dev.* 2012;26(9):877–890.
15. Le A, et al. Glucose-independent glutamine metabolism via TCA cycling for proliferation and survival in B cells. *Cell Metab.* 2012;15(1):110–121.
16. Gao P, et al. c-Myc suppression of miR-23a/b enhances mitochondrial glutaminase expression and glutamine metabolism. *Nature.* 2009;458(7239):762–765.
17. Liu W, et al. Reprogramming of proline and glutamine metabolism contributes to the proliferative and metabolic responses regulated by oncogenic transcription factor c-MYC. *Proc Natl Acad Sci U S A.* 2012;109(23):8983–8988.
18. Son J, et al. Glutamine supports pancreatic cancer growth through a KRAS-regulated metabolic pathway. *Nature.* 2013;496(7443):101–105.
19. Ying H, et al. Oncogenic Kras maintains pancreatic tumors through regulation of anabolic glucose metabolism. *Cell.* 2012;149(3):656–670.
20. Suzuki S, et al. Phosphate-activated glutaminase (GLS2), a p53-inducible regulator of glutamine metabolism and reactive oxygen species. *Proc Natl Acad Sci U S A.* 2010;107(16):7461–7466.
21. Qie S, Chu C, Li W, Wang C, Sang N. ErbB2 activation upregulates glutaminase 1 expression which promotes breast cancer cell proliferation. *J Cell Biochem.* 2014;115(3):498–509.
22. Csibi A, et al. The mTORC1 pathway stimulates glutamine metabolism and cell proliferation by repressing SIRT4. *Cell.* 2013;153(4):840–854.
23. Tanaka K, et al. Compensatory glutamine metabolism promotes glioblastoma resistance to mTOR inhibitor treatment. *J Clin Invest.* 2015;125(4):1591–1602.
24. Jeon YJ, et al. Regulation of glutamine carrier proteins by RNF5 determines breast cancer response to ER stress-inducing chemotherapies. *Cancer Cell.* 2015;27(3):354–369.
25. Qing G, et al. ATF4 regulates MYC-mediated neuroblastoma cell death upon glutamine deprivation. *Cancer Cell.* 2012;22(5):631–644.
26. Cohen A, Barankiewicz J, Lederman HM, Gelfand EW. Purine and pyrimidine metabolism in human T lymphocytes. Regulation of deoxyribonucleotide metabolism. *J Biol Chem.* 1983;258(20):12334–12340.
27. Sigoillot FD, Berkowski JA, Sigoillot SM, Kotsis DH, Guy HI. Cell cycle-dependent regulation of pyrimidine biosynthesis. *J Biol Chem.* 2003;278(5):3403–3409.
28. Lane AN, Fan TW. Regulation of mammalian nucleotide metabolism and biosynthesis. *Nucleic Acids Res.* 2015;43(4):2466–2485.
29. Rao GN, Church RL. Regulation of CAD gene expression in mouse fibroblasts during the transition from the resting to the growing state. *Exp Cell Res.* 1988;178(2):449–456.
30. Carrey EA. Phosphorylation, allosteric effectors and inter-domain contacts in CAD; their role in regulation of early steps of pyrimidine biosynthesis. *Biochem Soc Trans.* 1993;21(1):191–195.
31. Macallan DC, Fullerton CA, Neese RA, Haddock K, Park SS, Hellerstein MK. Measurement of cell proliferation by labeling of DNA with stable isotope-labeled glucose: studies in vitro, in animals, and in humans. *Proc Natl Acad Sci U S A.* 1998;95(2):708–713.
32. Neese RA, et al. Measurement in vivo of proliferation rates of slow turnover cells by <sup>2</sup>H<sub>2</sub>O labeling of the deoxyribose moiety of DNA. *Proc Natl Acad Sci U S A.* 2002;99(24):15345–15350.
33. Duncan BK, Miller JH. Mutagenic deamination of cytosine residues in DNA. *Nature.* 1980;287(5782):560–561.
34. Bernhard SA, Tompa P. The mechanism of succinate or fumarate transfer in the tricarboxylic acid cycle allows molecular rotation of the intermediate. *Arch Biochem Biophys.* 1990;276(1):191–198.
35. Li J, et al. Synthetic lethality of combined glutaminase and Hsp90 inhibition in mTORC1-driven tumor cells. *Proc Natl Acad Sci U S A.* 2015;112(1):E21–E29.
36. Adams DJ, et al. Discovery of small-molecule enhancers of reactive oxygen species that are nontoxic or cause genotype-selective cell death. *ACS Chem Biol.* 2013;8(5):923–929.
37. Gross MI, et al. Antitumor activity of the glutaminase inhibitor CB-839 in triple-negative breast cancer. *Mol Cancer Ther.* 2014;13(4):890–901.
38. Bester AC, et al. Nucleotide deficiency promotes genomic instability in early stages of cancer development. *Cell.* 2011;145(3):435–446.
39. Maréchal A, Zou L. DNA damage sensing by the ATM and ATR kinases. *Cold Spring Harb Perspect Biol.* 2013;5(9):a012716.
40. Merrick CJ, Jackson D, Diffley JF. Visualization of altered replication dynamics after DNA damage in human cells. *J Biol Chem.* 2004;279(19):20067–20075.
41. Ciccica A, Elledge SJ. The DNA damage response: making it safe to play with knives. *Mol Cell.* 2010;40(2):179–204.
42. Chou TC. Drug combination studies and their synergy quantification using the Chou-Talalay method. *Cancer Res.* 2010;70(2):440–446.
43. Tong X, Zhao F, Thompson CB. The molecular determinants of de novo nucleotide biosynthesis in cancer cells. *Curr Opin Genet Dev.* 2009;19(1):32–37.
44. Diebold I, Petry A, Hess J, Görlach A. The NADPH oxidase subunit NOX4 is a new target gene of the hypoxia-inducible factor-1. *Mol Biol Cell.* 2010;21(12):2087–2096.
45. Xiang Y, et al. Targeted inhibition of tumor-specific glutaminase diminishes cell-autonomous tumorigenesis. *J Clin Invest.* 2015;125(6):2293–2306.
46. Carey BW, Finley LW, Cross JR, Allis CD, Thompson CB. Intracellular  $\alpha$ -ketoglutarate maintains the pluripotency of embryonic stem cells. *Nature.* 2015;518(7539):413–416.
47. Ben-Sahra I, Howell JJ, Asara JM, Manning BD. Stimulation of de novo pyrimidine synthesis by growth signaling through mTOR and S6K1. *Science.* 2013;339(6125):1323–1328.
48. Lunt SY, et al. Pyruvate kinase isoform expression alters nucleotide synthesis to impact cell proliferation. *Mol Cell.* 2015;57(1):95–107.
49. Comerford SA, et al. Acetate dependence of tumors. *Cell.* 2014;159(7):1591–1602.
50. Yuneva MO, et al. The metabolic profile of tumors depends on both the responsible genetic lesion and tissue type. *Cell Metab.* 2012;15(2):157–170.
51. Cancer Genome Atlas Research Network. Comprehensive molecular characterization of clear cell renal cell carcinoma. *Nature.* 2013;499(7456):43–49.
52. Chakrabarti G, et al. Targeting glutamine metabolism sensitizes pancreatic cancer to PARP-driven metabolic catastrophe induced by  $\beta$ -lapachone. *Cancer Metab.* 2015;3:12.
53. Jacque N, et al. Targeting glutaminolysis has antileukemic activity in acute myeloid leukemia and synergizes with BCL-2 inhibition. *Blood.* 2015;126(11):1346–1356.
54. Bryant HE, et al. Specific killing of BRCA2-deficient tumours with inhibitors of poly(ADP-ribose) polymerase. *Nature.* 2005;434(7035):913–917.
55. Rouleau M, Patel A, Hendzel MJ, Kaufmann SH, Poirier GG. PARP inhibition: PARP1 and beyond. *Nat Rev Cancer.* 2010;10(4):293–301.
56. Juvekar A, et al. Combining a PI3K inhibitor with a PARP inhibitor provides an effective therapy for BRCA1-related breast cancer. *Cancer Discov.* 2012;2(11):1048–1063.
57. Helleday T. Putting poly (ADP-ribose) polymerase and other DNA repair inhibitors into clinical practice. *Curr Opin Oncol.* 2013;25(6):609–614.
58. Yuan M, Breitkopf SB, Yang X, Asara JM. A positive/negative ion-switching, targeted mass spectrometry-based metabolomics platform for bodily fluids, cells, and fresh and fixed tissue. *Nat Protoc.* 2012;7(5):872–881.
59. Jackson DA, Pombo A. Replicon clusters are stable units of chromosome structure: evidence that nuclear organization contributes to the efficient activation and propagation of S phase in human cells. *J Cell Biol.* 1998;140(6):1285–1295.